Preoperative planning and intraoperative image fusion improvement during endovascular aneurysm repair

Stefan P.M. Smorenburg

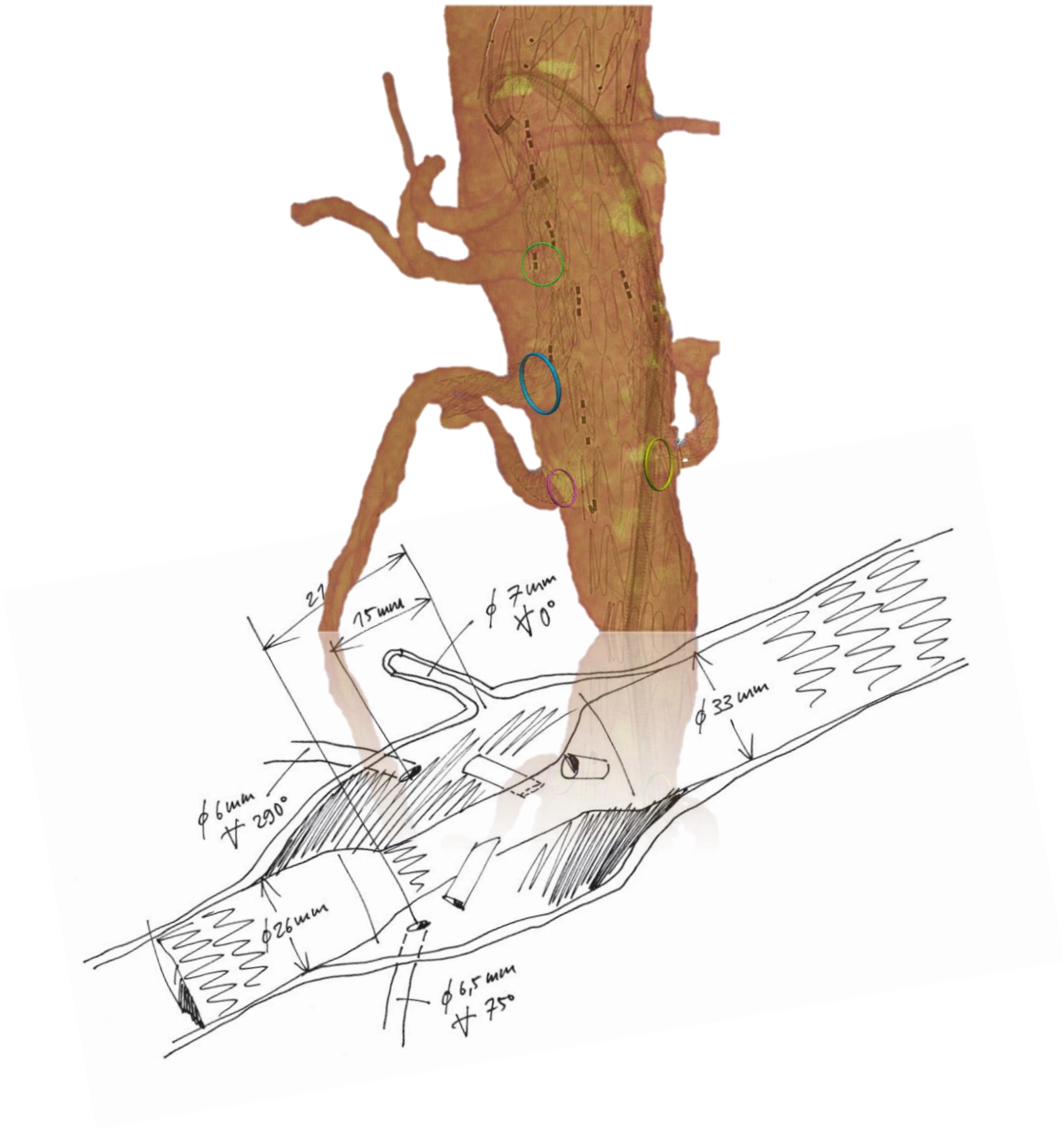

MSc. Graduation Committee:

Chairman	Prof. dr. ir. C.H. Slump[1]
Medical supervisor	Dr. A.W.J. Hoksbergen[2]
Technical supervisor UT	Prof. dr. ir. C.H. Slump[1]
Supervisor profession behaviour	Drs. E.M. Walter[1]
External member	J.K. van Zandwijk, MSc[1]
Additional member	I. Smit-Ockeloen, MSc[3]

1 *Technical Medicine, University of Twente, Enschede, the Netherlands*
2 *Department of Surgery, Amsterdam UMC, location VU University Medical Centre, Amsterdam, the Netherlands*
3 *Image Guided Therapy Systems - Innovation, Philips, Best, the Netherlands.*

27-11-2019
Version 1.3

Correspondence:
Stefan P.M. Smorenburg
s.smorenburg@amsterdamumc.nl

TABLE OF CONTENTS

PREFACE

After one year of work I present my final thesis. Many years have passed since I started with Technical Medicine in 2011. Who would have thought I would end up exactly where I feel at my place, on the hybrid operating room with innovative solutions and an energetic team at the Vascular Surgery department at Amsterdam UMC. I would like to thank my official and unofficial supervisors Arjan, Kakkhee, Kees, Elyse and Annelotte for their guidance the past year. My thesis will be the end product of a moving year in which I have gathered unforgettable national and international experiences with my new colleagues, which I am very proud of.

READING GUIDE

General abstract starts with a global introduction abstract of the general aim of the study. Since the thesis exist of two phases, more detailed abstracts will be presented before each phase. **Chapter 1** gives the clinical introduction of the patient disease, treatment and complications. **Chapter 2** answers these clinical complications and challenges by introducing a technical solution and explaining this technique. **Chapter 3** elaborates on the development of the suggested technique and its clinical use. **Chapter 4** states the research aim and research questions. **Chapter 5** presents the article and abstract of phase one concerning the preoperative planning improvement during EVAR. **Chapter 6** presents the article and abstract of phase two concerning the evaluation of automated fusion software. **Chapter 7** suggests the clinical implementation of the techniques. **Chapter 8** presents a proof of concept resulting from the recommendations of chapter 6. **Chapter 9** gives the general conclusion and **Chapter 10** elaborates on recommendations and future research.

GENERAL ABSTRACT

Objective: To improve endovascular aneurysm repair (EVAR) preoperative planning by evaluating automated and manual 3D sizing measurements in two software programs and to improve automated image fusion registration

Methods: A total of 40 patients with abdominal aortic aneurysms (AAA) treated with EVAR were retrospectively studied. Two study phases were defined. Phase one comprised EVAR preoperative planning and phase two comprised EVAR intraoperative image fusion of preoperative CTA and live fluoroscopy.

During phase one, 30 patients were measured on aortoiliac diameters and lengths with two software programs following a standardized measuring protocol consisting of 23 measurements per patient. Three investigators were defined: two vascular surgeons with over ten years surgery and sizing experience and one technical physician. Absolute measurements (mm) and interclass correlation coefficients (ICC) were obtained and inter-observer variability was calculated. Also the measurements were timed.

During phase two, 10 patients were evaluated with automated fusion software. An automated fusion prototype was developed with Philips (Best, the Netherlands). Preoperative computed tomography angiography (CTA) was fused with live fluoroscopy with the registration algorithm. Bone mismatch (mm) and vascular mismatch was measured (mm) and the registrations were timed.

Results: For phase one, 1380 measurements were performed. ICC values of 0.95 or higher were reached for all manual measurements. The automated measurements resulted in lower ICC.

For phase two, seven of the ten patients were fused fully automatically and three patients needed manual adjustment. A submillimetre bony mismatch was reached and a vascular mismatch of >5 mm.

Conclusions: During preoperative planning, manual measurements have an almost perfect agreement when measured in two different software programs. Automated measurement agreement is lower. Additionally, automated fusion was successful with a submillimetre bony mismatch.

1. CLINICAL INTRODUCTION

1.1. Clinical context

Abdominal aortic aneurysm (AAA) is an irreversible localized dilation of the abdominal aorta exceeding an anteroposterior diameter of ≥ 3.0 cm.[1, 2] AAA is often asymptomatic and the detection coincidental. In the Netherlands, approximately 2000 elective repairs of AAA are performed each year.[3, 4]

AAA classification is as follows, (i) suprarenal if the aneurysm extends above the origo of the renal arteries, (ii) pararenal if the aneurysm extends to the level of one or more renal arteries, (iii) juxtarenal if the aneurysm originates immediate distally of the renal arteries and (iv) infrarenal if the aneurysm originates distally to the renal arteries. The most important risk factors are smoking, older age, male gender and family history. [5]

Endovascular or open surgical repair are indicated in patients with an aneurysm diameter larger than 5.5 cm. If left untreated, the aneurysm can rupture which causes death in 75-80%.[2,3] Aneurysms below 5.5 cm are treated conservatively with regular ultrasound checkups and secondary prevention of cardiovascular morbidity.[6]

1.2. Treatment

Open surgery requires a large abdominal incision, after which a synthetic graft is sutured in the aneurysm, functioning as a new vessel. Endovascular aortic repair requires a small incision in the groin, after which a guidewire, catheter and stent graft are introduced in the abdominal aorta through the iliac arteries. Using fluoroscopy, the stent graft is visualized and placed in the abdominal aorta.

EVAR has become the preferred treatment option compared to open repair due to its minimal invasive character and lower risk of mortality and morbidity.[6] EVAR-1 and the Dutch DREAM trial have reported a 2.5-fold lower 30-day operative mortality compared with open repair at 6 months.[4] Long-term survival is similar between open and endovascular. However reintervention rates are higher after EVAR exceeding values of 20% after one year and 40% after 12 years due to the possibility of developing endoleaks with the chance of aneurysm rupture.[7-9]

Stent graft devices have evolved from standard configurations, to custom-made more flexible stent grafts incorporating branches, fenestrations and scallops.[10,11] These developments make the endovascular treatment of complex cases such as suprarenal, pararenal and juxtarenal AAA possible and expands the indication for EVAR. The fenestrations, branches and scallops in the stent graft fabric enable extension of the sealzone to a healthier part of the aorta. Also, challenging anatomical configurations such as an absent, short or angulated proximal neck can now be treated with EVAR.[12]

During fenestrated endovascular aortic repair (FEVAR), the surgeon aligns the fenestrations of the stent graft with the origo of the aortic sidebranches: celiac artery (CA), superior mesenteric artery (SMA), right renal artery (RRA) left renal artery (LRA). Smaller covered stents are deployed in the aortic sidebranches to connect the main graft and allow for continuous blood flow.[10] With branched endovascular aortic repair (BEVAR), the method is similar only the main stent graft contains branches, to which smaller covered stents are attached into the aortic sidebranches.[11] Figure 1 displays the branches and fenestrations.

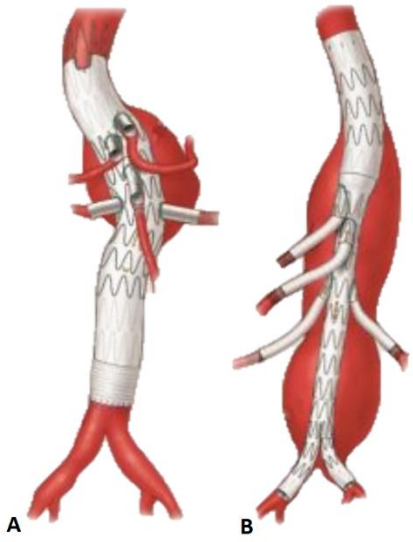

Figure 1 EVAR with fenestrations (A) and branches (B). *Image courtesy Oderich G. – Endovascular Aortic Repair, Chapter 2, 2017*

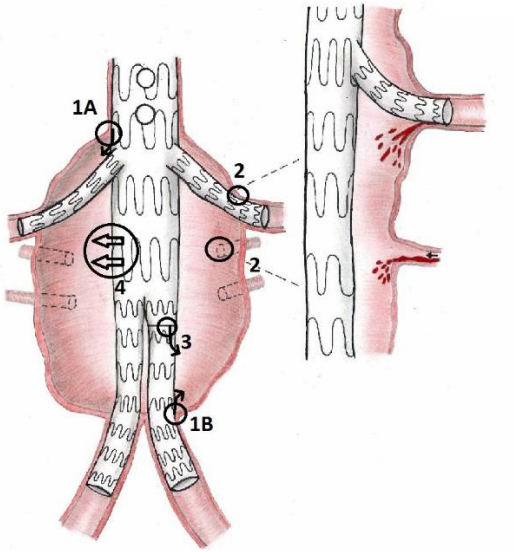

Figure 2 Proximal (1A) and distal (1B) endoleak, backflow endoleak (2), graft separation endoleak (3) and porosity endoleak (4). *Image courtesy LUMC Leiden - Behandeling van complexe aneurysma's met een stent, 2019.*

1.3. Planning

Technical success of EVAR falls or stands with adequate pre-operative planning and sizing.[12] 'Failing to plan is planning to fail' is an often heard adage in the world of vascular surgery.[13] The routine use of 3D preoperative sizing software for EVAR significantly reduces the rate of type 1 endoleaks.[14, 15] A central lumen line (CLL), is constructed intraluminal, which allows a longitudinal visualization of the aorta and tortuous segments. This ensures accurate length measurements between landing zones and anatomic targets such as the distance from the lowest renal artery to the internal iliac arteries.[16]

With custom-made stent graft configurations and the treatment of pararenal and suprarenal AAAs, preoperative planning is more technically demanding since the stent graft is sized on patient specific anatomies. A lack of sufficient planning and sizing is associated with the development of endoleaks, stent migration and sac expansion, requiring additional secondary reinterventions.[12]

1.4. Endoleaks

A disadvantage of EVAR is the occurrence of endoleaks and the higher rate of secondary interventions compared to open repair.[7, 17, 18] Figure 2 displays the different types of endoleaks. Endoleak type I indicates insufficient sealing at proximal (1a) or distal (1b) attachment sites of the stent graft. The incidence is up to 5% and treatment usually consists of implantation of additional stent grafts .[19] Endoleak type II is backflow via lumbar arteries or a patent inferior mesenteric artery. Incidence is 10-15% and can be treated conservatively, but when sac expansion is present usually embolization is performed.[19] Endoleak type III is the separation of stent graft components. Incidence is up to 4 % and treatment consists of placing a bridging stent graft.[19] Endoleak type IV is porosity in the graft material which is rare with new-generation devices. Stent graft migration is the caudal movement of the main body of the stent graft due to insufficient proximal seal. This can lead to type Ia endoleak. Incidence is up to 5% and treatment exists of placing additional stent grafts or fixation of the stent to the aortic wall with endoanchors.[19]

AAA is a progressive aortic disease regardless of the stent graft choice or type of surgery (open versus endovascular). Also, neck dimensions are not stable.[20-25] There is evidence that after EVAR, proximal aortic neck dilation occurs and neck enlargement continues to progress, even years after the initial procedure.[17] For the surgeon, it is important to acknowledge that aortic disease is progressive and precise EVAR planning can minimize late failures from type I endoleak or migration. A well-defined EVAR planning workflow ensures aortic diameters and lengths obtained from a CLL.

2. TECHNICAL INTRODUCTION

2.1. Image fusion

Fenestrated and branched EVAR can increase the procedure time, fluoroscopy time, radiation dose and nephrotoxic contrast up to 10 times compared to standard EVAR.[26-28] The main imaging modality in EVAR is X-ray fluoroscopy. A recent trend in EVAR imaging is image fusion. Image fusion merges pre-operative computed tomography angiography (CTA) of a patient with live fluoroscopy. This enables the surgeon to use the pre-operative CTA as a 3D roadmap. Currently, the aorta and vascular branches have always been imaged with digital subtraction angiography (DSA) which needs nephrotoxic contrast.[29-34] It has been reported in several articles that the advantage of image fusion is the reduction of nephrotoxic contrast and the reduction of fluoroscopy time during complex EVAR.[35-40]

The surgeon navigates the catheters with guidance of the pre-operative CTA which is superimposed on live fluoroscopy. A second feature of image fusion is that when the C-arm or table is moved lateral, medial, proximal or distal, the 3D roadmap moves in the same directions as the table and C-arm. This enables the surgeon to navigate to the desired region of interest without using extra fluoroscopy. A third feature of image fusion is that the C-arm angles of the artery ostia can be oriented pre-operatively, saved and recalled intraoperatively.[41]

In order to match the pre-operative CTA with live fluoroscopy, an accurate registration is needed. The registration of image fusion can be performed in two ways, as 2D-3D registration or as 3D-3D registration. With the 2D-3D method, two single-shot images are acquired intraoperatively, usually from the pelvic rims and vertebral column, with a minimum angular difference of ≥ 30°. After this, the pre-operative CTA is registered to the live fluoroscopy by using bony landmarks; the upper pelvis and vertebral column. This is performed manually during the operation.[29] Figure 3 displays the workflow steps needed for 2D-3D registration.

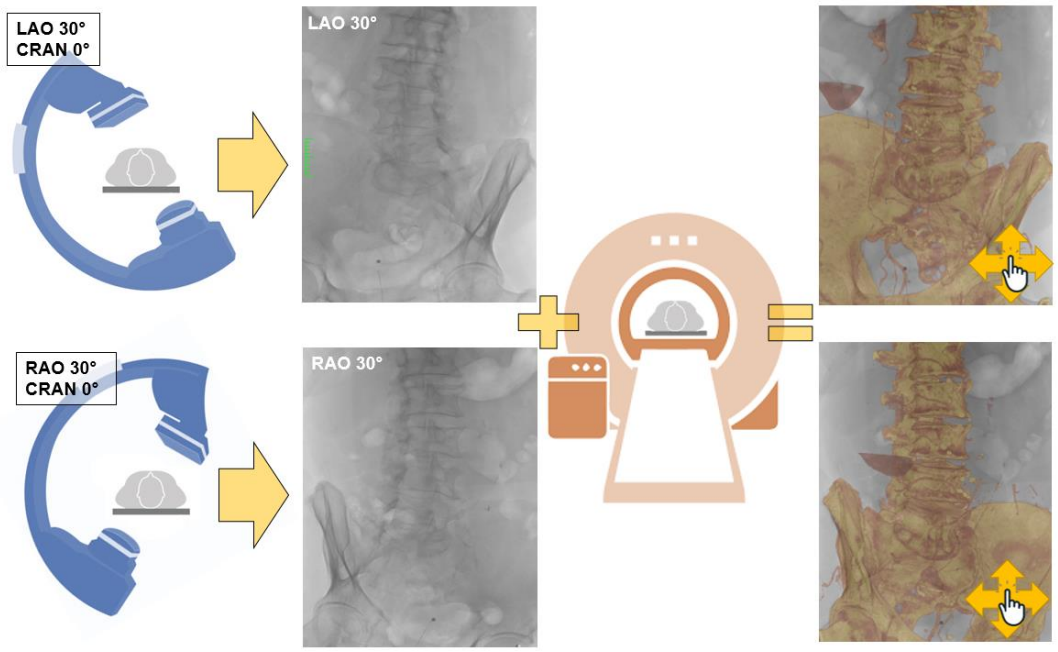

Figure 3 Workflow of the 2D-3D registration during image fusion. In this example, two fluoroscopy acquisitions at left anterior oblique (LAO) and right anterior oblique (RAO) are acquired at 30°. These images are fused with preoperative CTA (orange) manually by moving the preoperative CTA up/down/left/right to ensure a bone match.

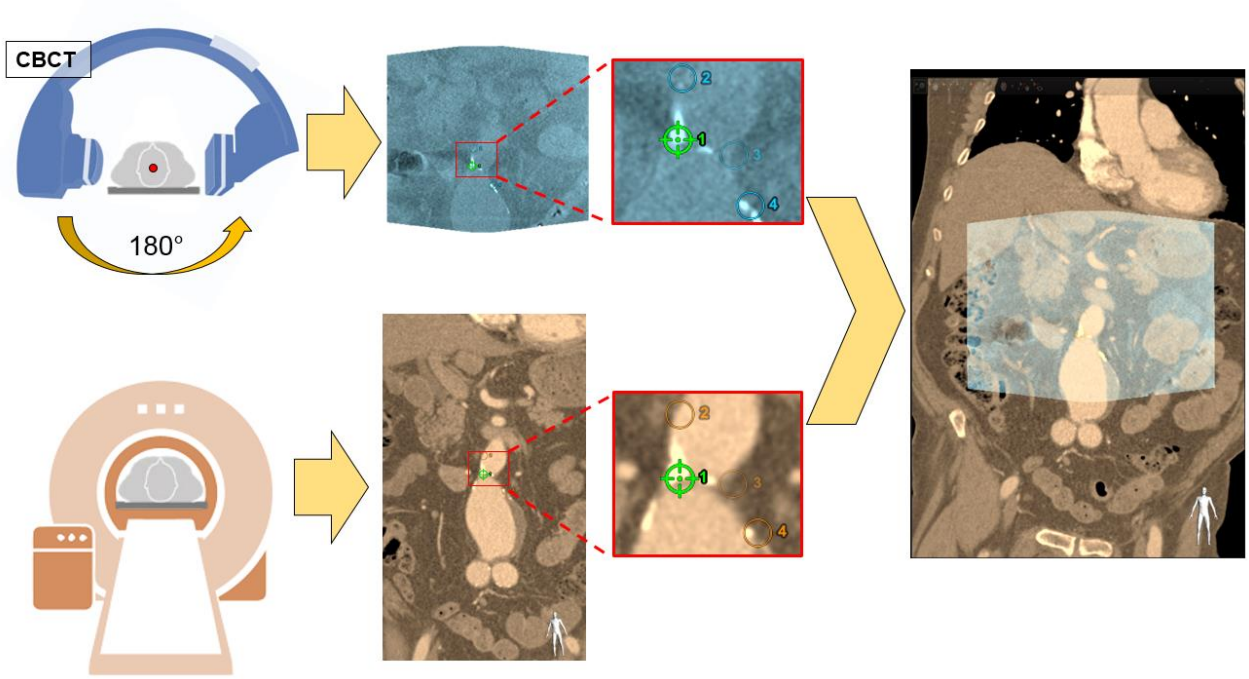

Figure 4 Workflow of the 3D-3D registration during image fusion. A cone beam CT (CBCT) is acquired intraoperatively by the C-arm following a 180° acquisition. Typically, 5 to 6 aortic calcifications are selected (red box) in both the CBCT and preoperative CTA (orange). This manual process fuses the preoperative CTA and CBCT in three dimensions.

With 3D-3D registration, a cone beam computed tomography (CBCT) is acquired intraoperatively. The C-arm follows a 180° circular trajectory which results in a 3D scan of the patients' abdomen. After this, the 3D scan is registered to the preoperative CTA by matching aneurysm calcifications. [29] Figure 4 displays the workflow steps needed for 3D-3D registration. The amount of radiation needed for the CBCT is in general equal to one DSA.[39] In normal EVAR, DSA is a large contributor to the total amount of radiation.

2.2. Image registration

Image registration is the alignment of points from one image to corresponding points in another image.[42] Images acquired from multiple modalities are geometrically aligned for effective observation. In recent years, many image registration algorithms and image registration strategies are proposed to address several clinical problems.[43]

In a typical image registration process, a moving image is aligned with a fixed image by a transformation model. Image registration is generally categorized into two groups, rigid registration and non-rigid registration.[44] Fixed structures in the human body such as bone, are suitable for rigid registration. The image transformation exists with 6 degrees of freedom, see Figure 5. This means the structure can translate (up, down, left, right), rotate (roll, pitch, yaw), scale (back, forward) + aspect ratio (width, height) + shear (shift).

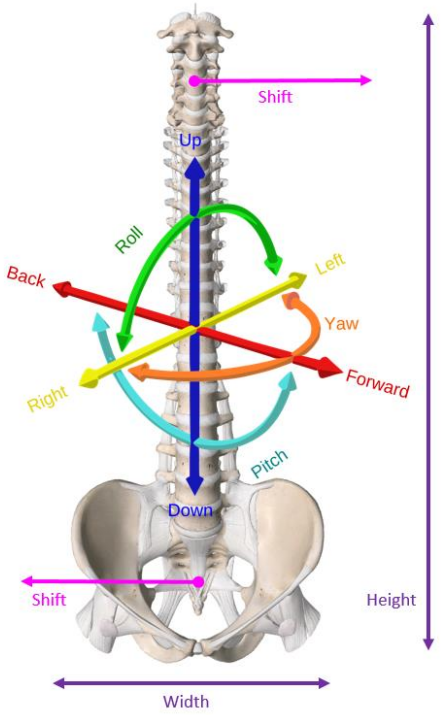

Figure 5 Vertebral column with 6 degrees of freedom affine transformation, the colors in the text correspond with the movements. *Image adapted from and courtesy of Essential Anatomy 4, 3D4DMedical, 2019.*

Non-rigid registration, or deformable image registration, is complicated since the correspondence between two images cannot be reached without local twisting image regions out of shape (warping).[45] A three dimensional pixel is defined as a voxel. With non-rigid registration, a displacement field is calculated at each voxel.

The development of non-rigid registration algorithms has become the main interest of medical image registration nowadays. Human tissue such as organs and vascular tissue is deformable and lends itself to deformable registration algorithms. Areas in which non-rigid image registration currently are used are in hepatic, prostatic and lung oncological surgery, to use image fusion in order to localize the tumor.[45]

3. DEVELOPMENT

3.1. Preoperative planning

In standard EVAR during clinical practice, not always a 3D sizing CLL is constructed in order to size the optimal stent graft, especially in acute cases. Instead, the 2D viewer from PACS is used to measure 2D dimensions in standard EVAR. If the main stent graft body is known, the iliac leg length sizing can be performed on the OR during EVAR. The radiopaque pigtail catheter functions as a measuring tool so the legs can be measured.

With complex EVAR, all CTA's are send to the company which produces the stent graft. These companies also perform the 3D sizing and preoperative planning. However for a surgeon to fully plan a complex EVAR with 3D sizing costs a lot of time, while the company can also perform the 3D sizing. In agreement with the surgeon the right stent graft is chosen and the surgeon re-measures the proposed graft plan however not always with CLL reconstruction. Any efforts to improve sizing time will hypothetically results in a broader adoption of 3D sizing software, especially if combined with image fusion planning software.

3.2. Image fusion

It is important to first know the current workflow and procedure outcomes of EVAR before one can improve the procedure. During the past year, I have been present at the OR and participated in EVAR preoperative planning and intraoperative workflow to experience the patient workup. Currently to utilize image fusion, the steps displayed in Figure 6 have to be performed.

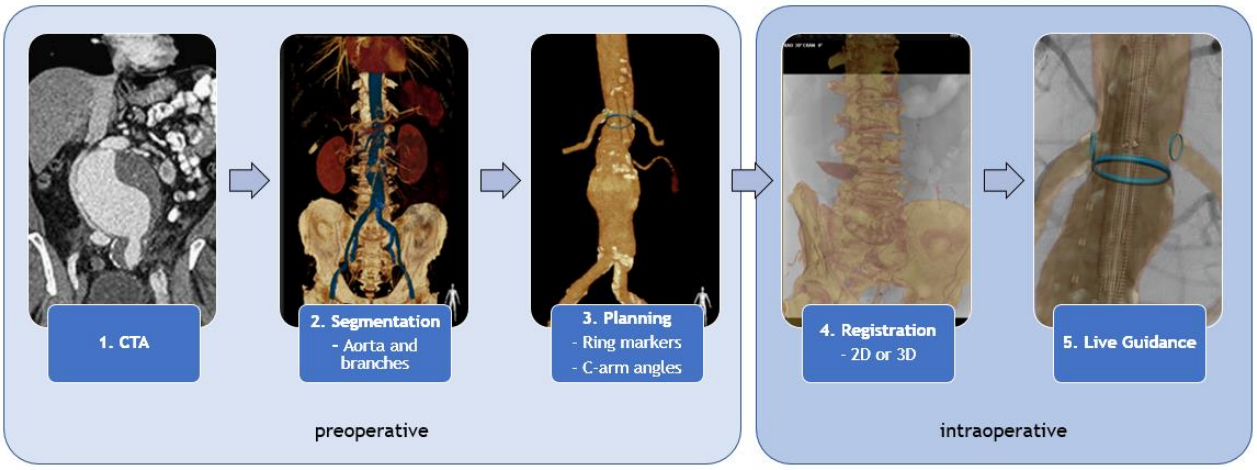

Figure 6 Current workflow steps to utilize image fusion during EVAR. It exists of importing the preoperative CTA (1) segment the aorta and branches (2), placing the navigation ring markers (3) manual registration of preoperative CTA with fluoroscopy (4) and live guidance (5).

As one can see all these steps have to be performed manually and if not practiced, this can take quite some time. At the start we were 20 minutes busy with image fusion preparations however we can currently perform it in around 15 minutes. Any improvements to upgrade these manual steps to automate will reduce the preparation time and can increase the accuracy. Figure 7 displays how image fusion is used in the operation room. On the large flexvision monitor, image fusion is projected next to the fluoroscopy image without fusion. During table and C-arm manoeuvres, the surgeons look to the fusion. Also during cannulation of the visceral arteries during complex EVAR the image fusion technology is helpful since no contrast is used to visualize the origo of the visceral arteries (Figure 7b).

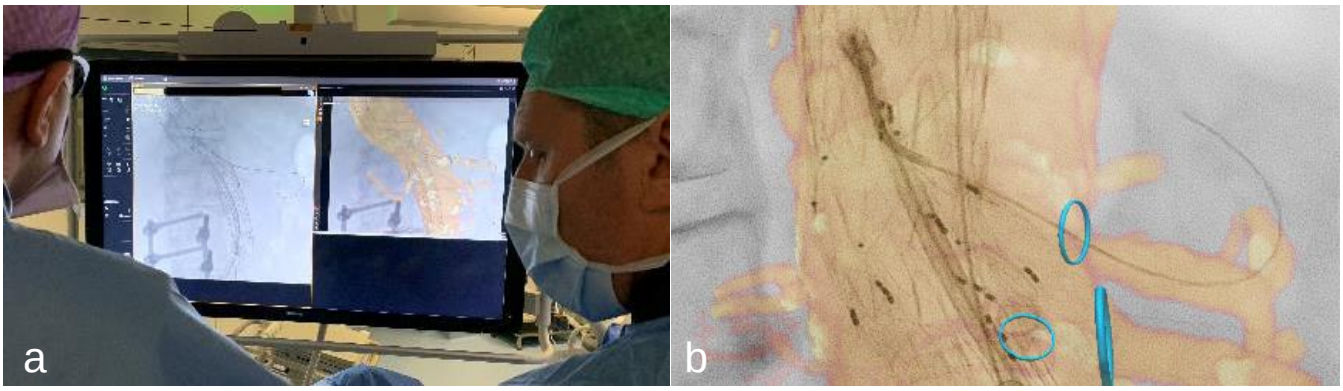

Figure 7 Monitor lay-out of image fusion during a procedure (a) and the cannulation of the celiac artery with the guidewire through the navigation marker (b).

Also, a current challenge of image fusion is the manual DSA correction which has to be performed mostly when using 2D-3D registration. We experienced that even with a good bone registration, still manual correction was needed. An example of the manual correction is displayed in Figure 8. A previous study performed at the department showed an image fusion mismatch of 6.1 mm. before manual DSA correction (Fig 8a). After manual DSA correction, the image fusion matches the DSA (Fig 8b). The iliac mismatch was measured in a previous study at 7.3 mm on average in 10 patients. This is due to the insertion of stiff guidewires and stiff endo stent devices. An example of this is displayed in Figure 8 mild (a) and sever (b). Furthermore, the preoperative planning for image fusion and 3D sizing has to be performed on separate workstations in our hospital.

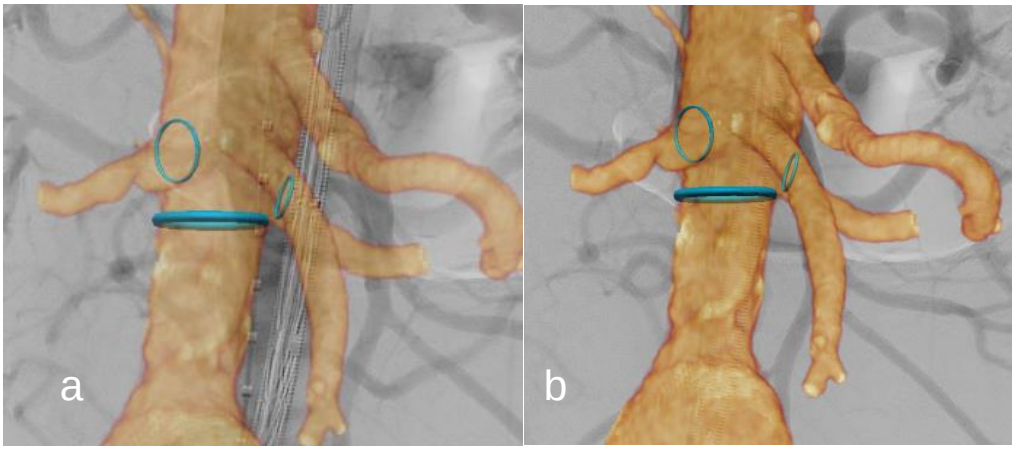

Figure 8 Manual correction after DSA. Image fusion mismatch (a) and image fusion match (b).

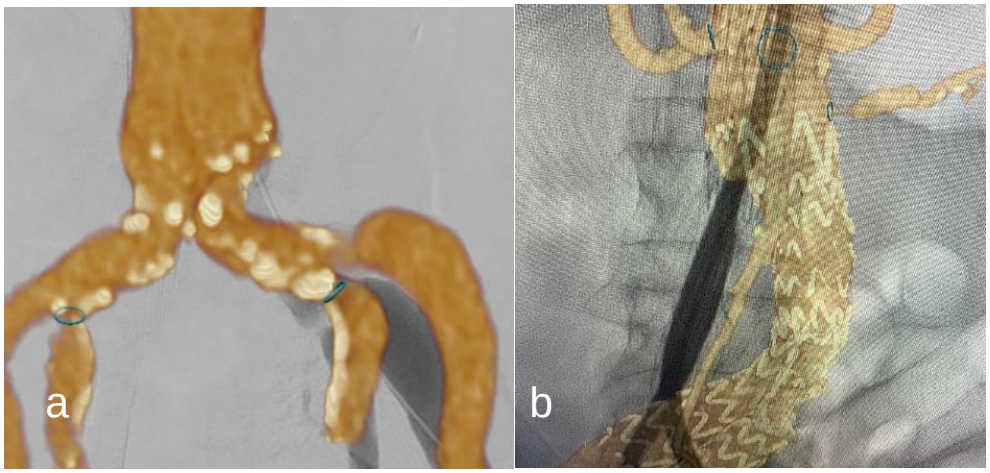

Figure 9 Iliac displacement mild (a) and severe displacement (b).

3.3. Procedural outcomes standard EVAR

EVAR outcome parameters can be obtained such as radiation dose; dose area product (DAP), Air Kerma (AK), fluoroscopy time, nephrotoxic contrast and procedure time. This data was collected in the development phase of this thesis for in total n=60 patients for standard EVAR between Jan 2017 and June 2018.

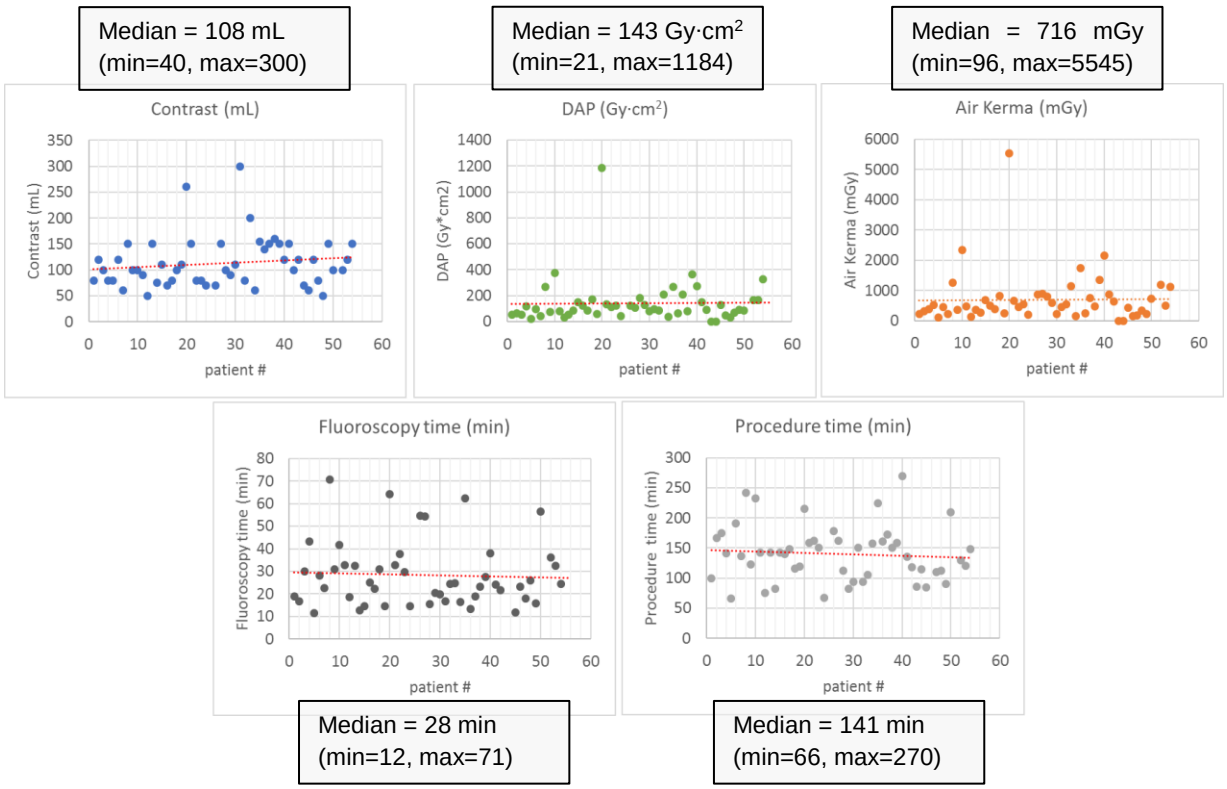

Figure 10 Procedural outcomes for standard EVAR at our hospital for contrast, DAP, Air Kerma, Fluoroscopy time and procedure time. The red trend line remains more or less constant.

Table 1 Literature for the comparison with our hospital data in standard EVAR.

Patients	Investigator	Year	Contrast (mL)	DAP	Air Kerma	Fluoroscopy time (min)	Procedure Time (min)
n=38	Herwaarden et al.[2]	2018	73	120	540	22	58
n=44	Maurel et al.[26]	2018	45	45	142	30	90
n=85	Hertault et al.[13]	2018	47	14.7	107	14	-
n=906	de Ruijter et al.[13]	2016	-	228	-	19	-

Figure 10 displays the procedural outcomes for standard EVAR. When comparing with literature, all literature values are lower compared with our hospital data. Note that these studies were published after they had implemented a radiation reduction protocol and other measures such as aggressive collimation. When comparing our results with older studies published in 2015/2016 the same values are reached.[35, 46]

3.4. Procedural outcomes complex EVAR

For the development phase of this thesis, procedural data was also obtained for complex EVAR to know what outcome values are currently reached during complex EVAR. De Ruijter et al. reported complex EVAR radiation dose can reach up to ten times the values compared with standard EVAR. [28]
Figure 11 displays the procedural outcomes for complex EVAR in our hospital. A cohort of patients from 2010-2016 was used with in total n=66 patients. Of all patients the procedure time was available. The contrast volume, DAP, Air Kerma and fluoroscopy time was only available of n=39 patients because of the utility of the new hybrid operation room.

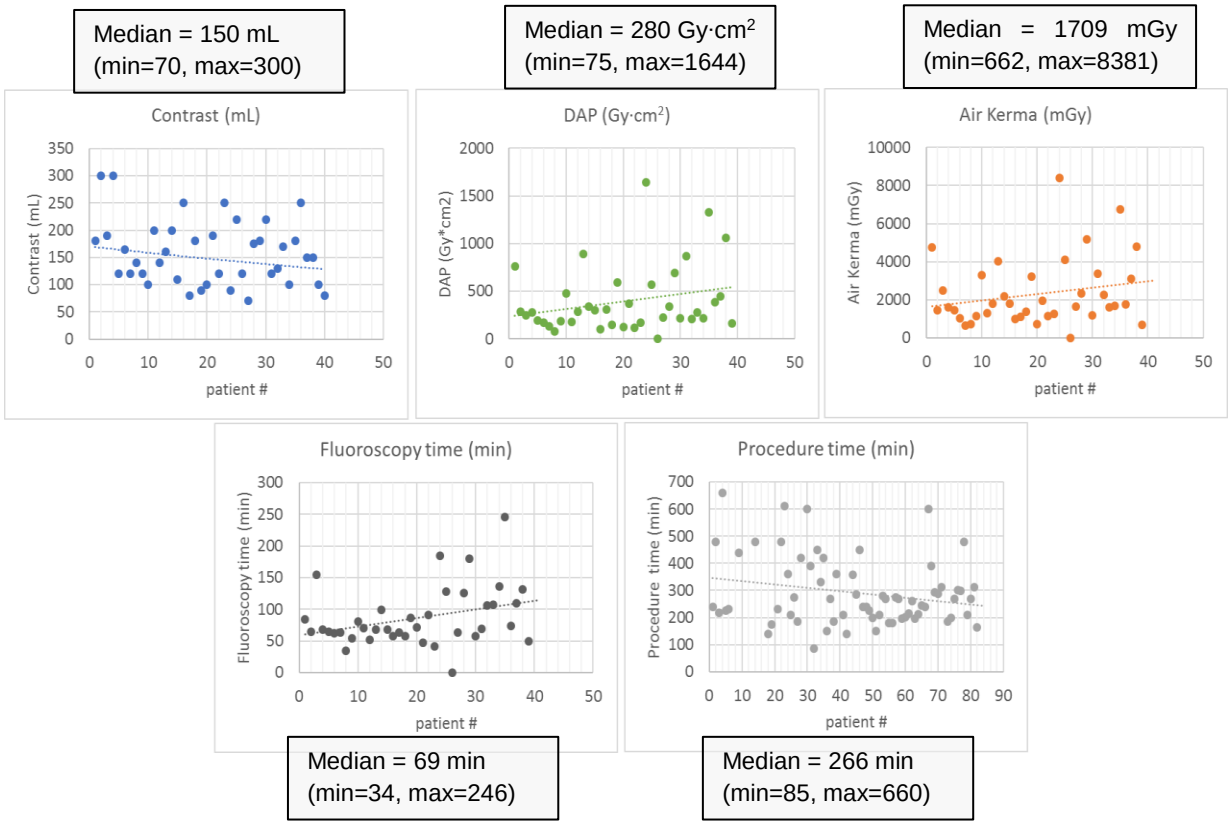

Figure 11 Procedural outcomes for complex EVAR at our hospital for contrast, DAP, Air Kerma, Fluoroscopy time and procedure time.

Table 2 Literature for the comparison with our hospital data in complex EVAR.

Patients	Investigator	Year	Contrast (mL)	DAP	Air Kerma	Fluoroscopy time (min)	Procedure Time (min)
n=288	Odericht et al[2]	2018	165	-	1709	88	260
n=24	Herwaarden et al.[26]	2018	172	362	2800	34	170

This resulted in a median contrast volume of 150 mL, median DAP of 280 Gy·cm², median air kerma of 1709 mGy, median fluoroscopy time of 69 min and median procedure time of 266 min as displayed in Figure 11. When comparing these values to the series by Oderich et al, similar values are found with minor differences. When comparing these values to the series of Herwaarden et al., we perform with lower DAP and air kerma however, their procedure time is shorter.
This thesis will not directly focus on implementing radiation reduction techniques such as collimation but will improve a radiation reduction technique called image fusion. The procedural values found in this development phase can be used as a control group in future studies after implementing image fusion with new capabilities such as automated registration.

4. AIM AND RESEARCH QUESTION

4.1. Problem context

The widespread adoption of 3D EVAR sizing software and intraoperative tools such as image fusion have enhanced the surgeons arsenal to improve EVAR patient outcome by reducing the rate of endoleaks, secondary interventions, operation time, radiation dose and nephrotoxic contrast. However, the implementation, usability and accuracy of these tools can be improved. First, when a surgeon chooses to use 3D sizing software and image fusion, double work is performed since both tools are on separate workstations and require the segmentation of the abdominal aorta. Also, all measurements have to be performed manually. Second, the 2D-3D registration of image fusion also has to be performed manually at the start of the EVAR procedure, this is subjective and potentially impedes optimal fusion match and is time-consuming.

4.2. General aim

To improve EVAR preoperative planning by evaluating automated and manual 3D sizing measurements and automated image fusion registration

4.3. Research question phase one

- What is the difference in automated and manual diameter and length measurements between new 3D sizing software of Philips (Advanced Vessel Analysis, Philips, Best, NL) (AVA) and TeraRecon (TR) (Aquarius iNtuition TeraRecon, San Mateo, CA, USA) during endovascular aneurysm repair planning?

Hypothesis:
The aortic measurements with AVA are expected to be just as precise compared to TeraRecon.

4.4. Research question phase two

What is the feasibility and precision of an automated registration algorithm during 2D-3D registration in image fusion?

Hypothesis:
Automated registration is expected to give a bone registration mismatch of <1 mm. It is expected to facilitate the ease of use of fusion imaging during EVAR procedures.

4.5. Articles

Both research questions are answered in the form of a scientific paper which is presented in the following pages.

Clinical evaluation of new sizing software on automated and manual sizing: Advanced Vessel Analysis (Philips) and Aquarius Intuition (TeraRecon)

Stefan P.M. Smorenburg[1,2], Maarten Truijers[1], Kak Khee Yeung[1], Arjan W.J. Hoksbergen[1]

Background: To evaluate the difference in terms of absolute outcome and inter-observer variability of aortoiliac measurements between two software programs applying automated and manual measurements.

Methods: A total of 30 patients (27 men, 3 women, mean age: 73.1 ± 7.3 years) with abdominal aortic aneurysms (AAA) treated with EVAR were retrospectively studied. A standardized measuring protocol comprising 23 measurements per patient was used existing of 4 automated and 4 manual inner-to-inner aortic diameters, 4 automated and 4 manual outer-to-outer aortic diameters, 3 manual aortoiliac lengths and 4 automated iliac inner-to-inner diameters. Measurements were performed with two software programs: Advanced Vessel Analytics (AVA) (Philips Healthcare, Best, NL) and TeraRecon (TR) (Aquarius iNtuition, Foster City, California, USA) by three investigators: two experienced vascular surgeons with >10y surgery and sizing experience and one technical physician. Primary endpoints were aortoiliac diameters and lengths (mm). Secondary endpoint was measurement time (min). Variability between the two software programs was assessed with intraclass correlation coefficients (ICC) and inter-observer user variability between the investigators was assessed with ICC and Bland-Altman. Additionally, a Hounsfield (HU) analysis was performed to analyse the automated measuring functionality. Also, an aneurysm AAA model with known dimensions was scanned and measured with both software programs to assess the measurement accuracy.

Results: Comparison of the two software programs demonstrated an excellent agreement for manual outer-to-outer measurements (min ICC = 0.95, max ICC = 0.97) and aortic lengths (min ICC = 0.97, max ICC =0.98). Fair agreement was observed for automated inner-to-inner diameters (min ICC = 0.68, max ICC = 0.87) and between automated outer-to-outer (AVA) and manual outer-to-outer (TR) diameters (min ICC = 0.49, max ICC = 0.59). Inter-observer variability was excellent (min ICC=0.97, max ICC= 0.98). HU analysis showed intraluminal values between 100-350 HU. The AAA model validation demonstrated a mean difference of 0.4 ± 0.31 mm for TR and 0.3 ± 0.3 mm for AVA.

Conclusions: AVA is as precise as TR for lengths and manual outer-to-outer diameters. For automated inner-to-inner, AVA is less accurate compared to TR.

[1]Department of Surgery, Amsterdam UMC, location VU University Hospital, Amsterdam, the Netherlands.

[2]Department of Technical Medicine, Techmed Centre, Twente University, Enschede, the Netherlands

Correspondence: s.smorenburg@amsterdamumc.nl

5.1. Introduction

Endoleaks and reintervention are the Achilles heel of endovascular aneurysm repair (EVAR).[1-4] EVAR complication rates are high, 20% after one month and 40% in 12-years leading to aortic related reinterventions, based on the Dutch Randomized trial (DREAM).[5-8] Stent graft designs have improved but outcomes remain variable. Endoleaks can occur within a month or after years due to loss of sealing, enlargement of the neck or migration of the stent graft leading to further dilation of the AAA, which is then prone to rupture.[9]

Endoleak type I indicates insufficient sealing at the proximal or distal attachment sites of the stent graft. The incidence is between 2-5% and treatment consists of implantation of additional stent grafts.[8] Endoleak type II is backflow via lumbar arteries or a patent inferior mesenteric artery. Incidence is 10-15% at 6 months and can be treated conservatively, but when sac expansion is present usually embolization is performed.[8]

AAA is a progressive aortic disease regardless of the stent graft choice or type of surgery (open versus endovascular). Also, neck dimensions are not fixed. There is evidence that after EVAR, proximal aortic neck dilation occurs and neck enlargement continues to progress, even years after the procedure.[1] It is hypothesized that this is caused by the radial force of the stent graft however this remains uncertain.[18]

Precise EVAR planning is very important as it can minimize late failures from type I endoleak or migration. [10-13] Typically, EVAR planning is performed on a three-dimensional workstation (3DWS) based on preoperative CTA. Many 3DWS are commercially available of which Aquarius Intuition (TeraRecon, San Mateo, CA, USA) (TR) is our reference software program. Two types of diameter measurements can be obtained namely the inner-to-inner diameter; this comprises the intraluminal aorta from intima to intima including thrombus excluding calcifications and the outer-to-outer diameter; this comprises the aortic diameter of adventitia to adventitia including calcifications. When sizing a stent graft, a manufacturer depended worksheet is used to determine which stent graft is proposed for the patient. Worldwide, three brands of stent grafts are commonly used; Zenith Alpha by Cook Medical (Miami Lakes, FL, USA), Endurant by Medtronic (Minneapolis, MN, USA) and Gore Excluder by W.L. Gore (Flagstaff, FL, USA). The instructions for use (IFU) for the Zenith Alpha describe outer-to-outer vessel wall measurement and IFU of the Endurant and Excluder describe inner-to-inner vessel wall measurements.

For this study, we introduce new sizing software; Advanced Vessel Analysis (AVA) (Philips, Best, the Netherlands). Among vascular surgeons, this software is currently unfamiliar and has its existence in radiology. AVA can be integrated with image fusion software to ensure the use of a 3D roadmap. However before integration, an evaluation of AVA has to be performed. A comparison of AVA versus a well-established vascular 3DWS is absent in literature and the outcome unknown.

The aim of this study is to evaluate the accuracy of AVA by comparing it with TR during EVAR operation pre-planning.

5.2. Methods

This study was conducted with approval of the local ethics committee and GDPR guidelines. A total of 30 patients (27 men, 3 women, mean age, SD: 73.1 $\pm$ 7.3 years, BMI: 29.0 $\pm$ 5.0 kg/m^2) with abdominal aortic aneurysms (AAA) treated with EVAR were retrospectively studied. Primary endpoints were aortoiliac diameters and lengths (mm). Secondary endpoint was measurement time (min). Inclusion criteria were elective infrarenal EVAR patients. The number of subjects (n=30) is based on a power calculation (α= 0.150) with a two-sided 95% confidence interval.

Preoperatively, a CTA was acquired with scan settings: 512x512x~1000 voxels, slice thickness: 0.90 mm, voxel size: 1x1x0.9, 120 kV, 130 mAs. Iodine based contrast was administered with a power injector and volume of 100 mL, 5 mL/s, 300 mg I/mL (UltraVist; Bayer HealthCare AG, Berlin, Germany) with a 20 second delay.

CTA's were uploaded to a GDPR-secured cloud environment for both AVA and TR. Three investigators were selected for the study; one technical physician (observer one) and two experienced vascular surgeons with over ten years surgery and sizing experience (investigators two and three). All three

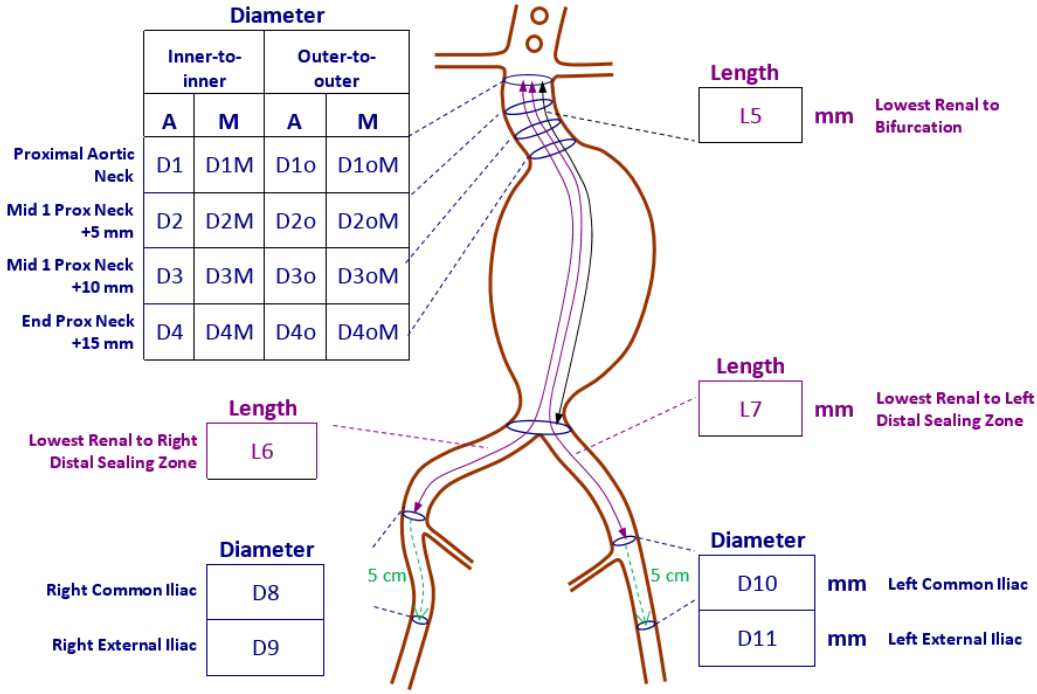

Figure 1 Standardized measurement protocol comprising 23 EVAR measurements. D1-D4 is measured automated and manual for both the inner-to-inner and outer-to-outer diameter. D5-D7 are manual lengths. D8-D11 are automated inner-to-inner iliac diameters.

investigators obtained a training session with both software programs of two hours with two test patients. A standardized measuring protocol was created comprising 23 measurements existing of 4 automated and 4 manual inner-to-inner aortic diameters, 4 automated and 4 manual outer-to-outer aortic diameters, 3 manual aortoiliac lengths and 4 automated iliac inner-to-inner diameters (Figure 1). Before measuring, a semi-automated central lumen line (CLL) was created for all patients by investigator one in TR and saved for later recall. AVA created a CLL fully automatically when the CTA was imported. After CLL creation, the trajectory was reviewed axially to ensure the seed point was in the centre of the aortic lumen.

Investigator one measured all 30 patients in both AVA and TR. Investigators two and three measured 15 patients with 8 measurements in TR to calculate inter-observer user variability. The order of patient presentation was random, and the investigators were blinded to each other and previous measurements. Measurements were performed on an identical hospital workstation with identical surrounding conditions. All measurements were performed once by each investigator. TR and AVA offer both automated inner-to-inner diameter measurements. Automated outer-to-outer measurements is only offered by AVA and not by TR. In total 4 comparisons were made in AVA and TR to ensure an elaborate comparison between both software programs and the manual and automated capabilities. Comparison 1: automated versus manual inner-to-inner aortic diameters. Comparison 2: automated versus manual outer-to-outer aortic diameters. Comparison 3: manual aortoiliac lengths. Comparison 4: automated iliac inner-to-inner diameters. Also, to determine inter-observer user variability, the measurements of both vascular surgeons were compared, and these results were compared with the measurements of the technical physician.

5.2.1. Statistical analysis

To obtain agreement between the aortic diameters and lengths from two different software packages, the intraclass correlation coefficient (ICC) is utilized (agreement, 2-way-mixed, single measure) and averaged over the measurement locations. An ICC of 1.0 equals with perfect agreement, ICC > 0.85 equals with an excellent agreement, ICC between 0.75-0.85 equals good agreement, ICC between 0.40-0.75 equals fair agreement and ICC < 0.40 equals poor agreement. Inter-observer variability was determined by ICC calculation

and Bland-Altman Analysis with 95% limits of agreement. P values <.05 were considered statistically significant. Statistical analyses were performed by using SPSS, Version 21 (IBM, Armonk, New York). Clinically relevant measurement mismatch was determined at > 2 mm. Manual inner-to-inner diameter measurements were performed in both TR and AVA. If absolute mean difference was <0.5 mm and ICC comparison >0.9 the measurements were averaged and defined as 'manual'.

5.2.2. Hounsfield analysis

Different tissue types correspond with specific pixel values defined as Hounsfield unit (HU) ranges. Both software programs offer an automated option, the inner-to-inner diameter which relies on HU classification. Additionally, a HU analysis is performed with a corresponding axial CTA slice to investigate the HU values which correspond with the intraluminal diameters according to the software program. Values are reported.

5.2.3. Validation with AAA model

An external validation with an AAA model gives an indication of the measurement accuracy. This is since the aortic dimensions of the AAA model are known, and the aortic dimensions of the patients are not known. Both TR and AVA were evaluated with an aneurysm AAA model for measurements D10 – D11. The same protocol was applied to the AAA as with the patients; a CTA was performed and measurements in TR and AVA obtained.

5.3. Results

In total, 1380 measurements were obtained in 30 patients by three investigators.

Comparison 1 existed of the automated versus manual inner-to-inner aortic diameters. The mean inner-to-inner values with standard deviations for TR, AVA and manual measurements are displayed in Table 1. The mean inner-to-inner outcome for AVA was 20.8 ± 3.0 mm, for TR 23.5 ± 3.3 mm and for manual 23.2 ± 3.0 mm. The mean difference and ICC between these measurements was calculated and displayed in Table 2. This resulted in a mean difference between AVA and manual measurements of 2.4 mm (p=.00) and an ICC of 0.69 corresponding with a fair agreement. The mean difference between TR automated and manual for the inner-to-inner measurements was 0.3 mm (p=.60) and an ICC of 0.92 corresponding with an excellent agreement.

Comparison 2 existed of the automated versus manual outer-to-outer aortic diameters. The mean outer-to-outer values with standard deviations for AVA and manual measurements are displayed in Table 3. The mean automated outer-to-outer diameter for AVA was 24.2 ± 3.6 mm and manual was 24.7 ± 2.8 mm. The mean difference and ICC was calculated and

Table 1 Mean inner-to-inner aortic diameters (mm) for AVA (yellow), TR (blue) and manual (red).

	Mean AVA automated (mm)	SD[a]	Mean TR automated (mm)	SD[a]	Mean manual AVA (mm)	SD[a]	Mean manual TR (mm)	SD[a]
D1	20.8	± 1.9	23.5	± 3.4	22.9	± 3.3	22.6	± 3.3
D2	20.5	± 3.5	23.4	± 3.4	23.2	± 3.1	23.1	± 3.2
D3	21.0	± 3.5	23.4	± 3.2	23.7	± 3.0	23.1	± 2.8
D4	20.9	± 3.1	23.8	± 3.1	23.9	± 2.9	23.5	± 2.8
Mean	**20.8**	± 3.0	**23.5**	± 3.3	**23.4**	± 3.0	**23.1**	± 2.9

Table 2 Comparison 1: inner-to-inner diameters automated and manual.

	AVA automated versus manual				*TR automated versus manual*				*AVA manual versus TR manual*	
	Mean difference[a] (mm)	**p[a]**	**ICC[b]**	**p[b]**	**Mean difference[a] (mm)**	**p[a]**	**ICC[b]**	**p[b]**	**ICC[b]**	**p[b]**
D1	2.0	.00	0.81	.00	0.7	.00	0.95	.00	0.90	.00
D2	2.6	.00	0.71	.00	0.3	.27	0.93	.00	0.94	.00
D3	2.4	.00	0.68	.00	0.0	.86	0.88	.00	0.92	.00
D4	2.8	.00	0.58	.00	0.1	.77	0.92	.00	0.89	.00
Mean	**2.4**	.00	**0.69**	.00	**0.3**	0.6	**0.92**	.00	**0.91**	.00

[a]Paired Sampled t-test

[b]Two way mixed, single measures

Table 3 Mean outer-to-outer aortic diameters (mm) for AVA (yellow) and manual (red). Note TR does not offer automated outer-to-outer functionality.

	Mean AVA automated (mm)	SD[a]	Mean manual AVA (mm)	SD[a]	Mean manual TR (mm)	SD[a]
D1	25.1	± 4.4	24.7	± 3.2	24.8	3.1
D2	23.8	± 3.7	24.6	± 2.8	24.7	3.0
D3	23.5	± 3.1	24.6	± 2.6	24.5	2.7
D4	24.2	± 3.2	24.9	± 2.7	24.8	2.7
Mean	**24.2**	± 3.6	**24.7**	± 2.8	**24.7**	± 2.8

Table 4 Comparison 2: outer-to-outer diameters automated and manual.

	AVA automated versus manual				*AVA manual versus TR manual*	
	Mean difference[a] (mm)	**p[a]**	**ICC[b]**	**p[b]**	**ICC[b]**	**p[b]**
D1	0.3	.69	0.50	.00	0.95	.00
D2	0.9	.13	0.57	.00	0.97	.00
D3	1.0	.04	0.57	.00	0.95	.00
D4	0.7	.21	0.55	.00	0.95	.00
Mean	**0.7**	.50	**0.50**	.00	**0.96**	.00

[a]Paired Sampled t-test
[b]Two way mixed, single measures

displayed in Table 4. This resulted in a mean difference of 0.7 mm (p=0.50) and an ICC of 0.50 corresponding with a fair agreement.

Comparison 3 existed of the manual aortoiliac lengths. The mean outer-to-outer values with standard deviations for AVA and manual measurements are displayed in Table 5. The mean manual length for AVA was 171 ± 14.0 mm and for TR 172 ± 18.3 mm. The mean difference result was 1.0 mm (p=0.40) and the ICC was 0.98 corresponding with a perfect agreement. Comparison 4 existed of automated iliac inner-to-inner diameters. The mean automated measurements with standard deviations are displayed in Table 6 The mean automated iliac inner-to-inner diameter for AVA was 10.3 ± 8.0 mm and for TR was 11.7 ± 3.5 mm. The mean difference result was 1.7 mm

Table 5 Comparison 3: manual aortoiliac lengths for AVA (yellow) and TR (blue). The mean difference and ICC is calculated (red) between the measurements of AVA and TR.

	Mean AVA (mm)	SD[a]	Mean TR (mm)	SD[a]	Mean difference[a] (mm)	p[a]	ICC[b]	p[b]
L5	133	± 3.2	133	± 13.3	0.3	.57	0.98	.00
L6	191	± 13.6	191	± 21.4	0.9	.25	0.98	.00
L7	190	± 22.0	191	± 18.5	1.7	.03	0.97	.00
Mean	**171**	**± 14.0**	**172**	**± 18.3**	**1.0**	**0.4**	**0.98**	**.00**

Table 6 Comparison 4: automated iliac inner-to-inner diameters for AVA (yellow) and TR (blue).

	Mean AVA (mm)	SD[a]	Mean TR (mm)	SD[a]	Mean difference[a] (mm)	p[a]	ICC[b]	p[b]
D8	13.1	± 19.6	15.2	± 4.9	2.1	.00	0.87	.00
D9	8.5	± 4.1	10.0	± 2.3	1.5	.00	0.76	.00
D10	12.6	± 2.0	14.8	± 4.0	2.2	.00	0.82	.00
D11	8.7	± 3.7	10.2	± 1.9	1.5	.00	0.68	.00
Mean	**10.3**	**8.0**	**11.7**	**3.5**	**1.7**	**.00**	**0.75**	**.00**

[a]Paired Sampled t-test
[b]Two way mixed, single measures

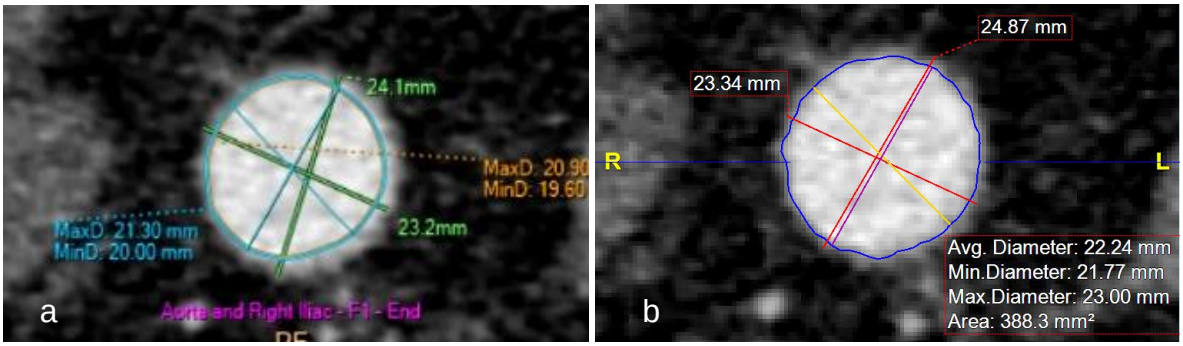

Figure 2 One measurement result for AVA (A) and TR (b). Note the difference in automated diameter outline of the lumen. In AVA, the iodinated aortic lumen exceeds the diameters shown by the program. *For more results see the Appendix.*

(p=.00) and the ICC was 0.75 corresponding with a good agreement.

One measurement result for both AVA and TR is displayed in Figure 2. The automated and manual outer-to-outer and inner-to-inner diameters is displayed.

5.3.1. Inter-observer user variability

The agreement between the two vascular surgeons was determined with manual outer-to-outer measurements and is displayed in Table 7. The mean difference between vascular surgeon one and vascular surgeon two was 0.2 ± 0.9 mm and an ICC of 0.98 (p=.00) corresponding with an almost perfect agreement. The measurements of the vascular surgeons was averaged and compared with the outer-to-outer manual measurements of the technical physician. This resulted in a mean difference of 0.3 ± 0.8 mm and an ICC of 0.98 (p=.00) corresponding with an almost perfect agreement. Additionally, Bland Altman agreement plots were created between the average of the vascular surgeons and technical physician which is displayed in Figure 6. All

Table 7: Inter-observer variability as mean difference and ICC of vascular surgeon 1 versus vascular surgeon 2. Also, the average of the surgeons versus the technical physician is displayed measured in TR.

	Vascular surgeon 1 versus vascular surgeon 2				*Vascular surgeons versus technical physician*			
	Mean difference[b] (mm)	**SD[b]**	**ICC[c]**	**p[c]**	**Mean difference[b] (mm)**	**SD[b]**	**ICC[c]**	**p[c]**
D1[a]	0.5	± 1.1	0.98	.00	0.3	± 0.75	0.99	.00
D2[a]	0.2	± 0.9	0.99	.00	0.3	± 1.1	0.97	.00
D3[a]	0.3	± 0.7	0.99	.00	0.1	± 0.7	0.98	.00
D4[a]	0.2	± 0.9	0.97	.00	0.4	± 0.5	0.99	.00
Mean	**0.2**	**± 0.9**	**0.98**	**.00**	**0.3**	**± 0.8**	**0.98**	**.00**

[a]Outer-to-outer, manual, [b]Paired-sampled T Test, [c]Two way mixed model, average measures

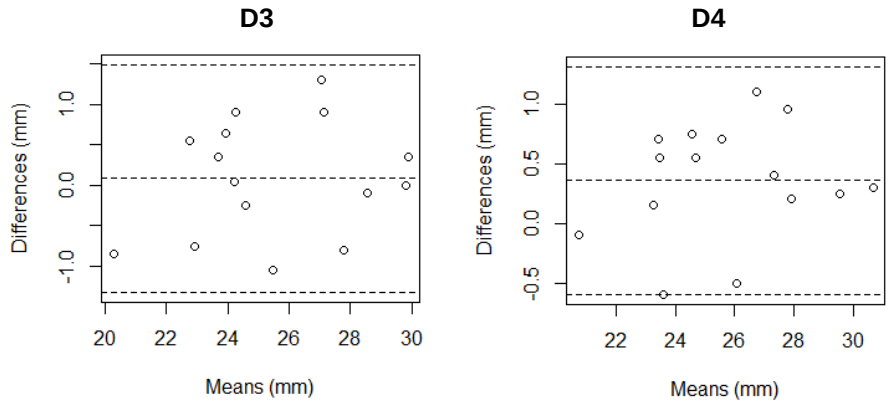

Figure 1 Bland-Altman agreement between the vascular surgeons and the technical physician for locations D3 and D4 manual outer-to-outer in TR. The line in the middle represents the mean difference, and the two dotted lines represent the upper and lower limits of agreement (mean difference ± 1.96 x standard deviation).

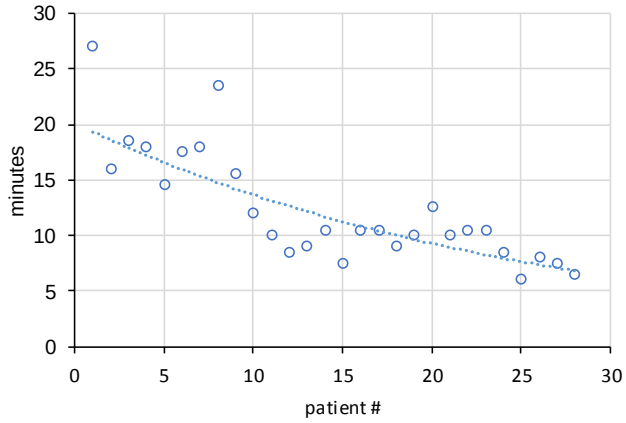

Figure 3 Measurement time per patient by investigator one utilizing one software program. Median time is 12.4 ± 4.4 min.

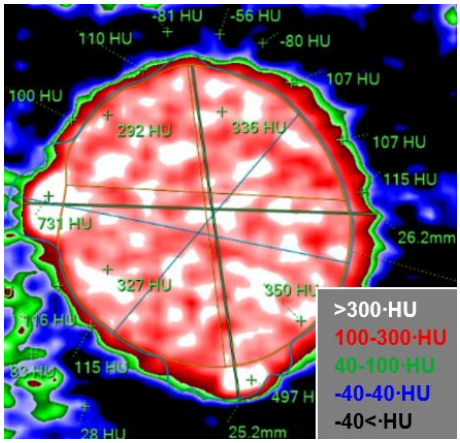

Figure 4 - Analysis of the vascular and surrounding pixel intensities in Hounsfield (HU) units with corresponding color legenda.

measurements of D3 and D4 are between the lower and upper agreement limits.

5.3.2.Measurement time

The measurement time decreased from a mean measurement time of 20 minutes per patient to a mean measurement time of 6 minutes per patient. The median measurement time was 12.4 ± 4.4 min for all patients. A learning curve can be observed in Figure 3 in which all the patients and their corresponding measurement times are displayed.

5.3.3. Hounsfield analysis

HU analysis reveals the HU values of the aortic proximal seal zone in Figure 4. Values >300 HU are in white, between 100-300 HU in red, between 30-100 HU in green, between -40-40 in blue and <40 HU in black.

Figure 4 reveals HU values between 292-731 HU in the intraluminal centre. Values between 100-116 HU are measured at the intraluminal edge, at the tunica intima. Values between 25-26 are measured in the vessel wall, at the tunica media. Outside the vessel wall values between -56-80 are measured, for various structures such as veins and surrounding tissue.

measurements of the external validation with the AAA model. Inner-to-inner diameters and outer-to-outer diameters were measured manual and automatically.

5.3.4. Validation with AAA model

Figure 5 displays the results of the validation with the AAA model. Measurements were obtained at iliac vessel corresponding with locations D11-D12 from the measurement protocol. The measurement accuracy of TR was 0.3 ± 0.3 mm and AVA was 0.4 ± 0.3 mm when comparing the measurements with the fixed AAA model dimensions.

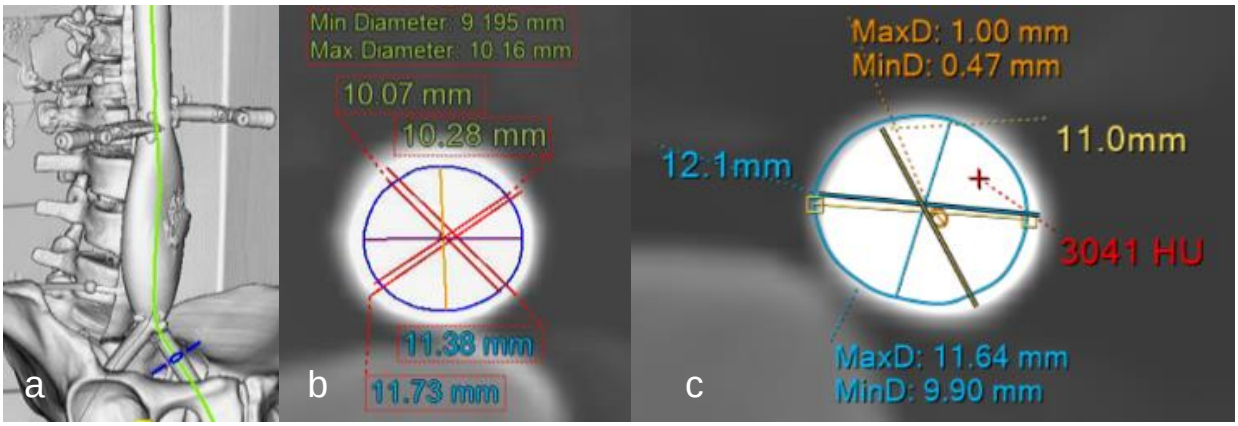

Figure 5 3D reconstruction (a) and measurements in TR (b) and AVA (c) Inner-to-inner and outer-to-outer diameters were automated and manual measured and compared with the fixed outer-to-outer diameter was 12 mm and fixed inner-to-inner diameter was 11 mm.

5.4. Discussion

The results above provide an overview of the evaluation and comparison of two software applications used for EVAR 3D sizing. Automated measurements and manual measurements were analysed.

The automated inner-to-inner measurements of AVA were on average 2.4 mm (p=.00) smaller compared to the manual inner-to-inner measurements resulting in a low ICC value of 0.69 (p=.00). In contrast, TR automated inner-to-inner mean difference was 0.3 ± 0.8 mm with an ICC of 0.92. AVA exceeded the clinically relevant measurement mismatch of >2mm. In automated inner-to-inner diameters. This difference can have large consequences when determining the right stent graft diameter in the aortic seal zone since under sizing can occur. The measurement example from Figure 2 measured 21 mm with AVA and 23 mm with TR. According to Gore Excluder IFU and AVA measurements, the aortic diameter is in the category of 19-21 mm which results in an aortic endoprosthesis diameter of 23 mm (oversizing of 10-20% is standard in all manufactures worksheets). However according to TR measurements (23 mm) the category of 22-23 should be used resulting in an aortic endoprosthesis diameter of 26 mm. Undersizing might result in more post-procedural complications such as endoleaks and stent migration so this is something that needs to be avoided in any case. Manual measurements between AVA and TR were almost perfect for inner-to-inner diameters.

Automated outer-to-outer measurements had a mean difference of 0.7 mm (p=.50) however a low ICC of 0.50 (p=.00). Figure 2A also displays the automated outer-to-outer measurement of AVA in blue. The application incorporates the calcifications in the measurements which is correct, however the edges of the vessel wall without calcifications are not included in the outer-to-outer measurements. This can also be seen in Figure 5 with extra Hounsfield (HU) analysis. In this example, an automated inner-to-inner (orange) and outer-to-outer (blue) measurement is performed. The difference between the measurements is only the incorporation of the two calcifications in the vessel wall, along the rest of the vessel wall the orange and blue line are on the same location, which is not correct since the outer vessel wall is on the outside of the light coloured iodine contrast. Manual measurements between AVA and TR were almost perfect for outer-to-outer diameters.

AVA versus TR manual lengths are comparable with ICC values reaching an almost perfect agreement.

Automated iliac inner-to-inner diameters resulted in an ICC of 0.75 corresponding with a good agreement however improvements can be made since the mean difference was 1.7 mm (p=.00) reaching almost the clinical relevant measurement mismatch of >2 mm.

The inter-observer variability was almost perfect between both vascular surgeons and between the vascular surgeons and the technical physician. The mean difference varied between 0.2-0.5 mm which was a submillimetre correspondence. The Bland-Altman showed all the measurements within the upper and lower agreement limits. The measurement time improved to 6 minutes per patients which is clinically acceptable.

Exploration of the HU-analysis in Figure 4 displays the main problem of the automated vessel analysis in AVA; the cutoff HU value to categorize intraluminal area seems too high. Structures at the edge of the vessel have a lower HU value and are still intraluminal however, not classified as such by AVA. Reports from literature suggests iodinated CTA corresponding with 100-600 HU.[14,15] These values are also found on the edges of the vessel in Figure 5 with HU values of 107-115, however these are not suggested as inner vessel by AVA. Calcifications correspond with >600 HU which is incorporated in AVA suggested by the blue outer-to-outer line. Muscle and soft tissue is categorized between 20-40 HU which could be used for the automated outer vessel measurements since the aortic media vessel wall exists of muscle tissue. However, this is a challenge since structures such as veins or other muscle tissue can be located adjacent to the vessel which might be a reason TR has not incorporated automated outer vessel wall measurements.

Validation with the AAA model showed a measurement accuracy of 0.4 ± 0.3 mm for AVA and 0.3 ± 0.3 for TR. This shows the

accuracy of the software programs is high since the measurement accuracy is below 0.5 mm.
Future research should focus on increasing the precision of automated sizing capabilities of sizing software. Currently too many manual steps and still manual sizing is needed for a correctly sized stent graft. This can also be seen in this study where all manual measurement comparisons resulted in an almost perfect agreement between software programs however not when automated measurements were incorporated except for the automated inner-to-inner diameters of TR. A manual check will be always needed, however, improving automated sizing capabilities may result in a higher precision comparable with manual sizing and decrease the sizing time in the pre-operative planning phase.

5.5. Conclusion

In the comparison between TR and AVA, the following conclusions can be drawn. All manual measurements resulted in an almost perfect agreement between both software programs. When utilizing automated measurements, the precision of TR was higher compared to TR.

References

1. Belvroy VM, Houben IB, Trimarchi S, Patel HJ, Moll FL, Van Herwaarden JA. Identifying and addressing the limitations of EVAR technology. *Expert Rev Med Devices* 2018; 15(8): 541-54.
2. Daye D, Walker TG. Complications of endovascular aneurysm repair of the thoracic and abdominal aorta: evaluation and management. *Cardiovascular Diagnosis and Therapy* 2018; (Suppl 1): S138-S56.
3. Kent KC. Clinical practice. Abdominal aortic aneurysms. *N Engl J Med* 2014; 371(22): 2101-8.
4. Sakalihasan N, Michel JB, Katsargyris A, et al. Abdominal aortic aneurysms. *Nature Review - Disease Primers* 2018; 4(1): 34.
5. Powell JT, Sweeting MJ, Ulug P, et al. Meta-analysis of individual-patient data from EVAR-1, DREAM, OVER and ACE trials comparing outcomes of endovascular or open repair for abdominal aortic aneurysm over 5 years. *Br J Surg* 2017; 104(3): 166-78.
6. Macia I, Grana M, Maiora J, Paloc C, de Blas M. Detection of type II endoleaks in abdominal aortic aneurysms after endovascular repair. *Comput Biol Med* 2011; 41(10): 871-80.
7. Kristmundsson T, Sonesson B, Dias N, Tornqvist P, Malina M, Resch T. Outcomes of fenestrated endovascular repair of juxtarenal aortic aneurysm. *J Vasc Surg* 2014; 59(1): 115-20.
8. Lu YH, Mani K, Panigrahi B, Hsu WT, Chen CY. Endoleak Assessment Using Computational Fluid Dynamics and Image Processing Methods in Stented Abdominal Aortic Aneurysm Models. *Comput Math Methods Med* 2016; 2016: 9567294.
9. Huang IKH, Renani SA, Morgan RA. Complications and Reinterventions After Fenestrated and Branched EVAR in Patients with Paravisceral and Thoracoabdominal Aneurysms. *Cardiovasc Intervent Radiol* 2018; 41(7): 985-97.
10. Sobocinski J, Chenorhokian H, Maurel B, et al. The benefits of EVAR planning using a 3D workstation. *Eur J Vasc Endovasc Surg* 2013; 46(4): 418-23.
11. Rolls AE, Riga CV, Rudarakanchana N, et al. Planning for EVAR: the role of modern software. *J Cardiovasc Surg (Torino)* 2014; 55(1): 1-7.
12. Velu JF, Groot Jebbink E, de Vries JP, Slump CH, Geelkerken RH. Validation of the Simbionix PROcedure Rehearsal Studio sizing module: A comparison of software for endovascular aneurysm repair sizing and planning. *Vascular* 2017; 25(1): 80-5.
13. Tinelli G, Hertault A, Martin Gonzalez T, et al. Evaluation of a new imaging software for aortic stent graft planning. *Eur Rev Med Pharmaco* 2017; 21(11): 2717-24.
14. Broder J. Diagnostic Imaging for the Emergency Physician - Hounsfield Scale: Saunders; 2011.
15. de Ruiter QM, Reitsma JB, Moll FL, van Herwaarden JA. Meta-analysis of Cumulative Radiation Duration and Dose During EVAR Using Mobile, Fixed, or Fixed/3D Fusion C-Arms. J Endovasc Ther. 2016;23:944-956.
16. de Ruiter QM, Gijsberts CM, Hazenberg CE, Moll FL, van Herwaarden JA. Radiation Awareness for Endovascular Abdominal Aortic Aneurysm Repair in the Hybrid Operating Room. An Instant Patient Risk Chart for Daily Practice. J Endovasc Ther. 2017;24:425-434.
17. de Ruiter QMB, Jansen MM, Moll FL, Hazenberg C, Kahya NN, van Herwaarden JA. Procedure and step-based analysis of the occupational radiation dose during endovascular aneurysm repair in the hybrid operating room. J Vasc Surg. 2018;67:1881-1890.
18. Southerland KW, Nag U, Turner M, et al. Image-Based Three-Dimensional Fusion Computed Tomography Decreases Radiation Exposure, Fluoroscopy Time, and Procedure Time During Endovascular Aortic Aneurysm Repair. *Journal of Vascular Surgery.* 2018;67:e61.
19. Kaladji A, Lucas A, Kervio G, Haigron P, Cardon A. Sizing for endovascular aneurysm repair: clinical evaluation of a new automated three-dimensional software. *Ann Vasc Surg.* 2010;24:912-920.
20. Greenberg R, Eagleton M, Mastracci T. Branched endografts for thoracoabdominal aneurysms. *J Thorac Cardiovasc Surg.* 2010;140:S171-178.
21. Wanhainen A, Verzini F, Van Herzeele I, et al. European Society for Vascular Surgery (ESVS) 2019 Clinical Practice Guidelines on the Management of Abdominal Aorto-iliac Artery Aneurysms. *European Journal of Vascular and Endovascular Surgery.* 2018.

6. PHASE TWO: AUTOMATED FUSION

Evaluation of Automated 2D-3D Bone Registration with Clinical Imaging Data to Improve Image Fusion: Feasibility Study

Stefan P.M. Smorenburg[1,2], Kak Khee Yeung[1], Arjan W.J. Hoksbergen[1]

Objective: To assess the feasibility and accuracy of an automated registration algorithm during 2D-3D registration which automatically fuses pre-operative CTA and live fluoroscopy.
Methods: A total of 10 patients (10 men, mean age: 75.6 ± 6.7, BMI: 31.6 ± 5.4 kg/m^2) with abdominal aortic aneurysms (AAA) treated with EVAR were retrospectively studied. Preoperative CTA and fluoroscopy of the procedure were analysed with new automated fusion software. The vertebral column was matched per vertebrae pair between pre-operative CTA and fluoroscopy. Automated rigid registration was performed by a registration algorithm to find an initial match (global) and second match (local). Primary outcomes were bony mismatch (mm), vascular mismatch (mm) after digital subtraction angiography (DSA) and a similarity score calculated by the software. Secondary outcomes were registration time (min) and vertebrae pair with the highest similarity score.
Results: In total, 60 registrations were performed with an average bony mismatch of 0.5 ± 0.6 mm, average vascular mismatch of 8.8 ± 5.5 mm and similarity score of 11% ± 3%. Automated registration was successful in 7 patients and manual help was needed in 3 patients.
Conclusions: The automated 2D-3D registration in image fusion is feasible with a submillimetre bony mismatch in the majority of the patients. Vascular mismatch still is large (>5 mm) and further improvement is advised.
Keywords: Image fusion, 2D-3D registration, 3D roadmap, EVAR, automated, navigation

6.1. Introduction

During endovascular aneurysm repair (EVAR) for abdominal aortic aneurysms (AAA), the surgeon guides guidewires and catheters through the femoral artery into the aorta with real-time X-ray guidance (fluoroscopy).[1-4]
A recently introduced technique is image fusion, which enables navigation of guidewires using a 3D vascular roadmap based on preoperative CTA. The 3D vascular roadmap is superimposed on the live fluoroscopy images during the procedure, making navigation more easy and exact.[29] The technique was introduced in 2015 by Schermerhorn et al. and revealed a reduction in radiation dose and contrast volume in complex EVAR.[5-11] Additional advantages are an optimal positioning of the C-arm angles to visualize renal and iliac arteries, which reduces the use of nephrotoxic contrast and radiation dose/exposure for the patient and medical staff.[36] However, the fusion between preoperative CTA and live fluoroscopy is performed by matching bony landmarks manually, making the technique operator-dependent, potentially hampering accuracy, and without experience the fusion can be

[1]*Department of Surgery, Amsterdam UMC, location VU University Hospital, Amsterdam, the Netherlands.*
[2]*Department of Technical Medicine, Techmed Centre, Twente University, Enschede, the Netherlands*
Correspondence: s.smorenburg@amsterdamumc.nl

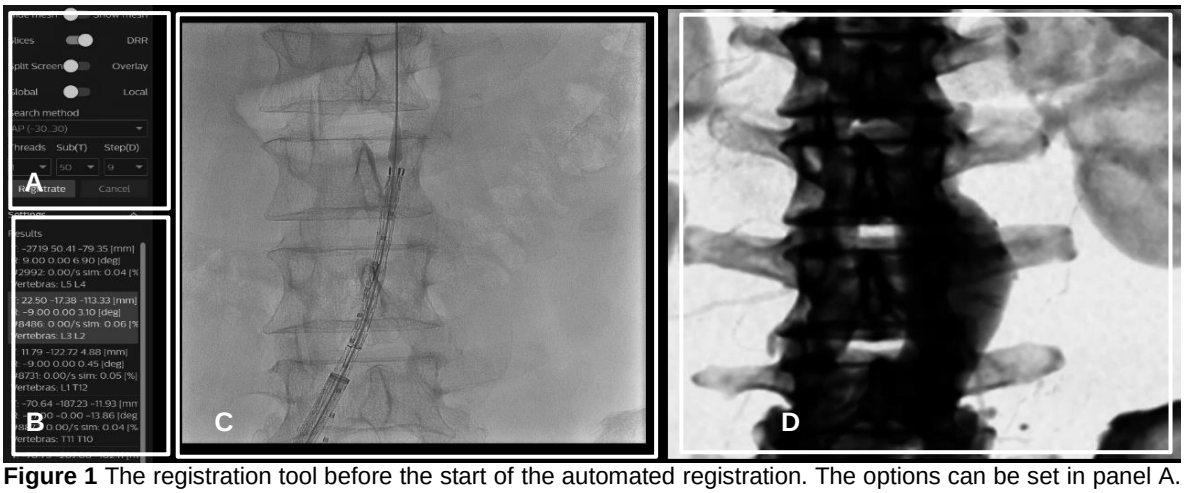

Figure 1 The registration tool before the start of the automated registration. The options can be set in panel A. The results are displayed in panel B. The first fluoroscopy of the initial angiography from the procedure is displayed in panel C and the preoperative CTA depicted as X-ray projection in panel D.

relatively time-consuming to perform. The aim of this study was to evaluate a new registration algorithm (Philips, Best, The Netherlands) on accuracy and feasibility which automatically fuses preoperative CTA and live fluoroscopy.

6.2. Methods

This study was conducted with approval of the local ethics committee and in accordance with GDPR guidelines. Preoperative anonymized CTAs and initial procedure DSA of 10 patients were used. CTA was acquired with scan settings: 512x512x~1000 voxels, slice thickness: 0.90 mm, voxel size: 1x1x0.9, 120 kV, 130 mAs. Iodine based contrast was administered with a volume of 100 mL, 5 mL/s, 300 mg I/mL (UltraVist; Bayer HealthCare AG, Berlin, Germany) with a 20 second delay.
For bone mismatch measurement, fluoroscopy is needed and for vascular mismatch measurement, digital subtraction angiography (DSA) was needed. DSA was acquired with 3 fps, low-dose abdomen protocol and utilization of the power injector with typically 20 mL, 15 mL/s, 300 mg I/mL. Primary outcomes were bony mismatch in mm, vascular mismatch in mm, and a similarity score. Bony mismatch was defined as the Euclidean distance of an identical anatomical vertebral location between preoperative CTA and fluoroscopy. Vascular mismatch was defined as the Euclidean distance of the ostium of the lowest renal artery between preoperative CTA and initial DSA. The similarity score was defined by the program. It calculates a similarity score based on edge matching of the vertebrae's which indicates the fusion success. A higher score corresponds with a better match. Additionally, the translation and rotation vectors in x,y,z were calculated. Secondary outcomes were registration time in min and vertebrae pair with highest similarity score. The type of study is retrospective.

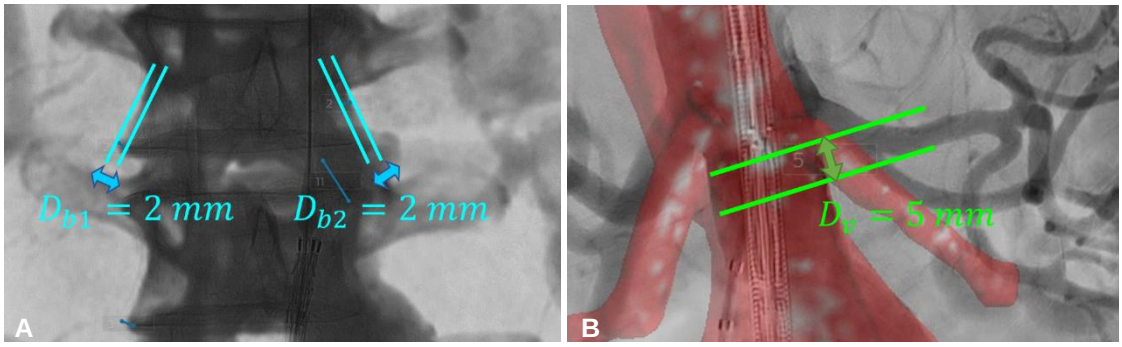

Figure 2 Bony mismatch (A) and vascular mismatch (B) measured in mm at the lateral side of the vertebral body and ostium displacement of the lowest renal artery respectively. Note that for the bony mismatch an average is calculated of the two results.

Table 1 Registration results for 10 patients. Displaying vertebrae-pair with highest similarity score (grey column), translation and rotation parameters (green column), bony mismatch and vascular mismatch (yellow column).

Patiënt	Global / Local	Similarity Score (%)	Vertebrae	Translation (pixels) T_x	T_y	T_z	Rotation (pixels) R_x	R_y	R_z	M_{bone} (mm)	$M_{vascular}$ (mm)
1	Global	0.06	L3-L2	22.50	-17.4	-113.33	-9.0	0.00	3.10	2	17
	Local	0.13	L5-L4	28.58	-14.6	-129.0	-5.7	-4.21	0.92	1	11
2	Global	0.05	L5 L4	1.36	-63.23	-84.37	-18.00	-8.91	2.62	3	7
	Local	0.11	L3 L2	-3.83	-66.0	-94.62	-20.36	-0.74	4.56	0	5
3	Global	0.09	L5 L4	23.52	-40.15	-112.5	-27.00	-26.73	6.10	2	16
	Local	0.10	L5 L4	18.75	-40.66	-111.7	-27.51	-24.27	6.51	0	14
4	Global	0.05	L5 L4	11.61	-74.82	-19.01	-27.00	-26.73	2.41	3	5
	Local	0.08	L5-L4	14.44	-74.21	-18.42	-26.47	-29.71	3.74	0	5
5	Global*	0.04	L3-L2	55.08	-22.42	49.54	-39.62	10.78	4.66	2	9
	Local*	0.04	L3-L2	55.08	-22.42	49.54	-39.62	10.78	4.66	2	9
6	Global	0.07	L1 T12	5.87	-13.0	-122.9	-9.00	8.91	2.00	3	3
	Local	0.13	L3 L2	8.23	-21.82	-119.8	-14.27	7.31	0.65	1	6
7	Global	0.07	L3 L2	4.59	-140.4	-61.75	-18.00	0.00	0.33	1	1
	Local	0.14	L5 L4	4.34	-43.46	-109.9	-21.26	-0.55	1.78	1	1
8	Global*	0.12	L1 T12	2.37	2.61	-227.2	-1.04	1.25	4.69	0	4
	Local*	0.12	L1 T12	2.37	2.61	-227.2	-1.04	1.25	4.69	0	4
9	Global	0.06	L5 L4	10.11	107.3	-167.8	9.00	000	-1.16	1	11
	Local	0.11	L3 L2	11.34	100.5	-172.2	1.36	-2.57	-0.49	0	18
10	Global*	0.08	L1 T12	-14.84	-18.51	-195.17	3.51	-2.75	0.54	1	17
	Local*	0.12	L5 L4	-15.15	-17.41	-198.5	-0.36	-2.98	0.29	1	15
Average Global		**0.07 ± 0.02**								**1.6 ± 0.9**	**9.0 ± 6.0**
Average Local		**0.11 ± 0.03**								**0.5 ± 6.6**	**8.8 ± 5.5**

*Manual help
M_{bone} = Mismatch bone
M_{vas} = Mismatch vascular

Inclusion criteria were elective infrarenal EVAR patients. The number of patients was n=10. One observer performed the mismatch measurements in the new fusion software version 1.0. Imaging data was imported into the new fusion software. The preoperative CTA was converted to X-ray projection fluoroscopy. Automated bone registration was performed on the patients vertebral column. First a global registration was performed, the global registration finds a global minimum in the pixel intensity. Second, a local registration was performed. The local registration has a smaller region of interest during the registration and finds a local minimum. The vertebrae pair with the highest similarity score was selected and this vertebrae pair was documented. Mismatch of fusion was determined by measuring the distance between an identical bone location in both CTA and fluoroscopy in mm. This was performed by placing manual anatomical markers on the vertebral body of each visible vertebra in both CTA and fluoroscopy. The Euclidean pixel distance was determined between these points in mm by using the calibrated diagnostic catheter as scale. Additionally, the vascular accuracy after fusion was determined by measuring mismatch of renal arteries (mm) between the vascular preoperative CTA and DSA after contrast injection at the renal ostium.

6.3. Results

Table 1 displays the numerical results of the automated registrations. In total, 60 registrations were performed of which the results with highest similarity scores are in Table 1. The average local bone mismatch was 0.5 ± 0.6 mm and global mismatch 1.6 ± 0.9 mm. The average local vascular mismatch was 8.8 ± 5.5 mm and global mismatch 9.0 ± 6.0

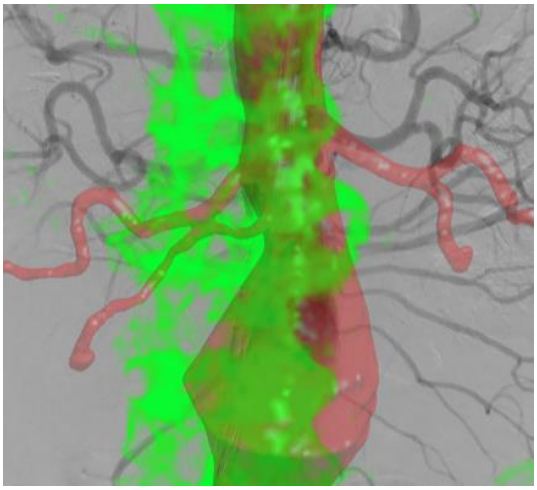

Figure 3 First DSA to confirm the origin of the renal artery displayed with the vertebral column (green) and image fusion (red).

mm. The average local similarity score was 11 % ± 3% and global similarity score 7% ± 2%. Bone mismatch varied between 0 and 3 mm while vascular mismatch varied between 1 and 18 mm. Vertebrae pair L5-L4 resulted in five patients with the highest similarity score. Vertebrae pair L3-L2 in four patients and L1-T12 in one patient with local registration. The similarity score and bone mismatch was always equal to or improved with local registration compared to global registration. The results of vascular mismatch were higher in patients 6 and 9 with local registration compared to global registration. Figure 3 displays an automated fusion result functioning as example. Figure 4 displays the time to perform the automated bone registrations. The median global time (mm:ss) was 13:46 (min=1:54 min, max=14:57 min) The median local time was 0:12 min (min=0:05 min, max=0:46). With patient 10, the software version was improved to version 1.1 and the fusion global time improved to 1:54 min.

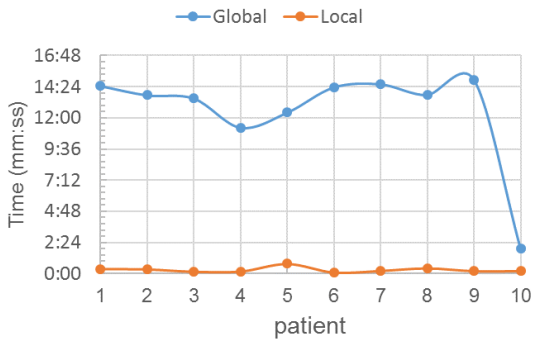

Figure 4 Time to perform the global and local registrations. For patient 10 a new version of the software was used and the registration time improved to 1:54 min.

6.4. Discussion

In this study, we have evaluated the feasibility and mismatch of automated registration with clinical patient images after EVAR. The overall mismatch after bone registration was submillimeter (0.5 ± 0.6 mm). Also, the average similarity score was 11 ± 3 % which can be improved even more. Automated registration was successful in 7/10 cases. Manual adjustments were needed in three cases, since there were several challenges varying from vertebrae's outside the field of view to a distorted image with many other structures present. *See the Appendix for these images.* The vascular mismatch was insufficient with an average mismatch of 8.8 ± 5.5 mm. One renal artery is on average 3-4 mm inner wall and 5-6 mm in diameter outer wall so this mismatch is clinical relevant. One of the causes of this mismatch is the vascular deformation introduced by a stiff guidewire, sheath and graft. Since this is retrospective obtained clinical data, these images represent real-world clinical cases in which this vascular deformation occurs. Having a registration algorithm with submillimetre mismatch on bone but an >5 mm mismatch vascular mismatch cannot be used which demonstrates the need for further development. In clinical practice, this mismatch can be corrected manually after DSA however this can impede the workflow and adding another manual step to the image fusion process.

When comparing global and local registration, an interesting phenomena is observed. With bone mismatch, the similarity score and accuracy measurements result in better outcomes due to the extra local registration after a global first search, improving from 7 ± 2% to 11 ± 3% and improving mismatch from 1.6 ± 0.9 mm to 0.5 ± 0.6 mm. This trend is not present during vascular mismatch measurements, since this resulted in 9.0 ± 6.0 mm for global and 8.8 ± 5.5 mm for local registration. The reason for this can be the vascular deformation introduced by the guidewire and stent delivery systems. In the current automated fusion software, this vascular deformation is not corrected.

The main challenge is not only a technical correct registration but also correct clinical implementation. The vision is that automated fusion occurs in the background and the operator does not have to interact with the image fusion. During clinical implementation, the registration algorithm will register on the first anterior-posterior X-ray image of the vertebral column presented during the procedure. This can be during the introduction of a floppy guidewire into the aorta.

However, if too many user interactions are needed and the registration takes a long time, automated registration will not be superior compared to manual registration.

One of the limitations is that this evaluation was performed with retrospective DSA images of the procedure. In clinical practice, image fusion is needed and can be helpful before the first DSA typically during the first introduction and navigation of the guidewires. Also before DSA, the diagnostic catheter is placed in the aorta right above the renal arteries. Image fusion can be helpful since the pigtail catheter can be placed with guidance of fusion images. During this study, we only could use fluoroscopy images after the introduction of a stiff guidewire and stent device, which causes vascular deformation and has consequences on the vascular mismatch. For further development, a prospective study is proposed in which the registration is performed on the first X-ray image available during the EVAR procedure. The system will propose an initial registration directly. Vascular mismatch can be determined by performing an DSA with only a floppy pigtail catheter placed in the aorta, without stiff guidewire and stiff delivery device. For research purposes, this could demonstrate the vascular mismatch without possible vessel displacement. In daily practice, an initial DSA is always performed with the stent device intraluminal, right before stent deployment which is why these images were used given the retrospective nature of the study.

Also, the time to perform automated registration is currently unsatisfactory (14 minutes). This can be improved by enhancing the computing power which was present in patient 10 (2 minutes).

It is important to continue the automated image fusion with vascular re-registration since in clinical setting the renal arteries are the starting point in stent graft placement. If image fusion presents a mismatch at this location, the surgeon's won't trust the software. Additionally, correcting for vascular deformity at the iliac trajectory is recommended. This can be performed by an iterative process. For example, the guidewire is detected, if the guidewire moves outside the preoperative fusion, it will correct automatically to morphologically deform the fusion to the guidewire since the guidewire is the standard and inside the patient.

6.5. Conclusion

In this study we have demonstrated that automated fusion between preoperative CTA and live fluoroscopy is feasible with a submillimetre bone mismatch. Vascular mismatch is insufficient (>5 mm). Future research should focus on the correction of the vascular mismatch.

References

1. *Koelemay M. Richtlijn 'Diagnostiek en behandeling van het aneurysma van de abdominale aorta'. Nederlands Tijdschrift Geneeskunde 2009.*
2. *Kent KC. Clinical practice. Abdominal aortic aneurysms. N Engl J Med 2014;371:2101-8.*
3. *Jones DW, Stangenberg L, Swerdlow NJ, et al. Image Fusion and 3-Dimensional Roadmapping in Endovascular Surgery. Ann Vasc Surg 2018;52:302-11.*
4. *Sakalihasan N, Michel JB, Katsargyris A, et al. Abdominal aortic aneurysms. Nature Review - Disease Primers 2018;4:34.*
5. *Ahmad W, Obeidi Y, Majd P, Brunkwall JS. The 2D-3D Registration Method in Image Fusion Is Accurate and Helps to Reduce the Used Contrast Medium, Radiation, and Procedural Time in Standard EVAR Procedures. Ann Vasc Surg 2018;51:177-86.*
6. *de Ruiter QM, Reitsma JB, Moll FL, van Herwaarden JA. Meta-analysis of Cumulative Radiation Duration and Dose During EVAR Using Mobile, Fixed, or Fixed/3D Fusion C-Arms. J Endovasc Ther 2016;23:944-56.*
7. *Goudeketting SR, Heinen SGH, Unlu C, et al. Pros and Cons of 3D Image Fusion in Endovascular Aortic Repair: A Systematic Review and Meta-analysis. J Endovasc Ther 2017;24:595-603.*
8. *Kaladji A, Dumenil A, Mahe G, et al. Safety and accuracy of endovascular aneurysm repair*

without pre-operative and intra-operative contrast agent. Eur J Vasc Endovasc Surg 2015;49:255-61.

9. *McNally MM, Scali ST, Feezor RJ, Neal D, Huber TS, Beck AW. Three-dimensional fusion computed tomography decreases radiation exposure, procedure time, and contrast use during fenestrated endovascular aortic repair. J Vasc Surg 2015;61:309-16.*
10. *Stangenberg L, Shuja F, Carelsen B, Elenbaas T, Wyers MC, Schermerhorn ML. A novel tool for three-dimensional roadmapping reduces radiation exposure and contrast agent dose in complex endovascular interventions. J Vasc Surg 2015;62:448-55.*
11. *Koutouzi G, Sandstrom C, Roos H, Henrikson O, Leonhardt H, Falkenberg M. Orthogonal Rings, Fiducial Markers, and Overlay Accuracy When Image Fusion is Used for EVAR Guidance. Eur J Vasc Endovasc Surg 2016;52:604-11.*
12. *Ahmad W, Obeidi Y, Majd P, Brunkwall JS. The 2D-3D Registration Method in Image Fusion Is Accurate and Helps to Reduce the Used Contrast Medium, Radiation, and Procedural Time in Standard EVAR Procedures. Ann Vasc Surg. 2018;51:177-186.*
13. *Liu Z, Deng X, Wang G-z. Accuracy Validation for Medical Image Registration Algorithms: a Review. Chinese Medical Sciences Journal. 2012;27:176-181.*
14. *Matl S, Brosig R, Baust M, Navab N, Demirci S. Vascular image registration techniques: A living review. Med Image Anal. 2017;35:1-17.*
15. *Fitzpatrick JM, West JB, Maurer CR, Jr. Predicting error in rigid-body point-based registration. IEEE Trans Med Imaging. 1998;17:694-702.*
16. *Raj Varadhan1, a, Grigorios Karangelis2, Karthik Krishnan3, and Susanta Hui4. A framework for deformable image registration validation in radiotherapy clinical applications. J Appl Clin Med Phys. 2013.*
17. *Truijers M, Resch T, Van Den Berg JC, Blankensteijn JD, Lonn L. Endovascular aneurysm repair: state-of-art imaging techniques for preoperative planning and surveillance. J Cardiovasc Surg (Torino). 2009;50:423-438.*
18. *Lessard S, Kauffmann C, Pfister M, et al. Automatic detection of selective arterial devices for advanced visualization during abdominal aortic aneurysm endovascular repair. Med Eng Phys. 2015;37:979-986.*
19. *Breininger K, Albarqouni S, Kurzendorfer T, Pfister M, Kowarschik M, Maier A. Intraoperative stent segmentation in X-ray fluoroscopy for endovascular aortic repair. Int J Comput Assist Radiol Surg. 2018;13:1221-1231.*
20. *Kaladji A, Dumenil A, Castro M, et al. Prediction of deformations during endovascular aortic aneurysm repair using finite element simulation. Comput Med Imaging Graph. 2013;37:142-149.*
21 Belvroy VM, Houben IB, Trimarchi S, Patel HJ, Moll FL, Van Herwaarden JA. Identifying and addressing the limitations of EVAR technology. *Expert Rev Med Devices.* 2018;15:541-554.
22. Huang IKH, Renani SA, Morgan RA. Complications and Reinterventions After Fenestrated and Branched EVAR in Patients with Paravisceral and Thoracoabdominal Aneurysms. *Cardiovasc Intervent Radiol.* 2018;41:985-997.
23. Lu YH, Mani K, Panigrahi B, Hsu WT, Chen CY. Endoleak Assessment Using Computational Fluid Dynamics and Image Processing Methods in Stented Abdominal Aortic Aneurysm Models. *Comput Math Methods Med.* 2016;2016:9567294.

7. IMPLEMENTATION

The (clinical) implementation of a new medical technique must not be underestimated. A technique with high expectations can still fail if careful implementation involving all stakeholders is not pursued.

In this report, the development of two existing techniques were evaluated; pre-operative 3D sizing software and image fusion. Figure 12 displays both techniques with 3D sizing in blue and image fusion in orange. This is the current situation in which all steps have to performed manually in the preoperative planning phase.

The goal is to automate all these steps, to shorten the preoperative planning time, standardize the individual steps and eventually improve the accuracy of the stent placement resulting in a longer lasting EVAR, with less radiation and contrast. In this study, the first steps were taken to automate steps 4 (measurements & registration) of Figure 12.

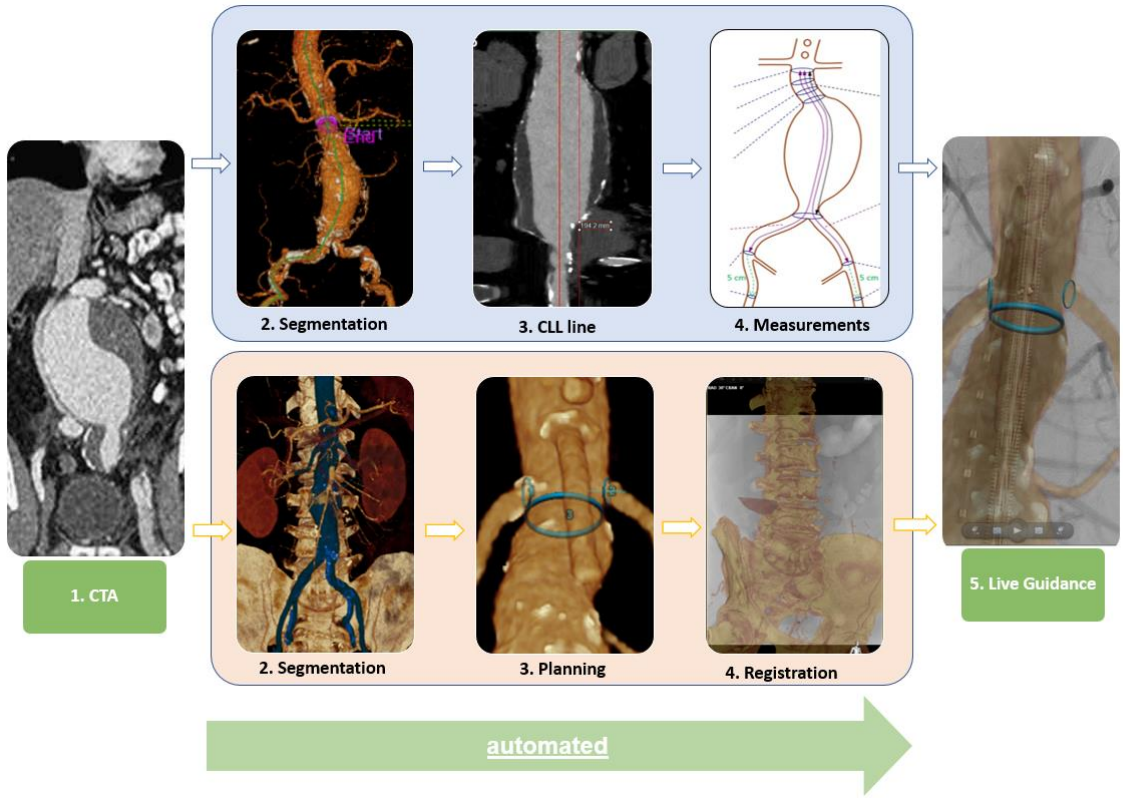

Figure 12 Overview of the steps leading to a live guidance with a correctly sized stent graft. To achieve 3D sizing (blue), segmentation, a CLL line and correct measurements are needed. To achieve image fusion (orange), segmentation, ring marker/C-arm planning and registration are needed.

The vision and optimal implementation of these techniques is as following:

- The physician sends the preoperative CTA to the EVAR planning module. The module then automatically calculates:
    - Aortoiliac segmentation, CLL line, measurements (diameters & lengths), image fusion navigation markers and optimal C-arm angles for the renal/iliac arteries. The physician corrects were needed.
- At the start of the procedure after percutaneous or cut-down groin access, the fusion of preoperative CTA with fluoroscopy is automatically achieved in the background with the first fluoroscopy images. An iterative registration process will run in the background to correct for vascular deformity and fusion mismatch.

8. PROOF OF CONCEPT

The vascular accuracy of the phase two study resulted in an average mismatch of 8.8 ± 5.5 mm. The recommendation following this was to perform a re-registration after the initial DSA. To investigate this, the automated re-registration (deformable fusion) was performed as a proof of concept principle.

8.1. Methods

An initial DSA (20 mL, 15 mL/s, 300 mg I/mL (UltraVist; Bayer HealthCare AG, Berlin, Germany) and image fusion result was used as starting point, see Figure 13 a,b. These images were loaded into Matlab R2019a (Mathworks, Natick, Massachusetts, United States) and toolboxes 'Color Thresholder', 'Image Segmenter' and 'Registration Estimator' were used.

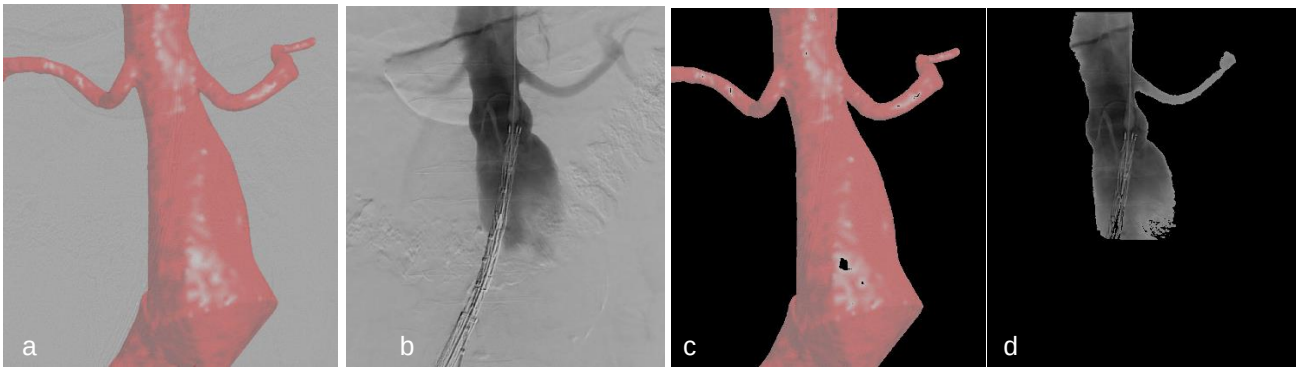

Figure 13 – Image fusion input separated as preoperative CTA (a) and initial DSA (b). Isolated preoperative CTA (c) and isolated DSA (d)

The following steps were taken: color thresholding to isolate the red pre-operative CTA (Figure 6c), thresholding to isolate the aorta in the DSA (Figure 6d). Also morphological operations to clean up the image were performed. The isolated images were loaded into the Registration Estimator Toolbox and affine non-rigid registration (deformable) was performed with a varying number of iterations (25-100) with stepsize 25. Also the Pyramid levels was varied between 6-10 and stepsize 2. The quality and time (sec) was reported and the vascular mismatch (mm) was measured at the renal artery ostium.

8.2. Results

Figure 14 displays the re-registration results of the improved fusion images.

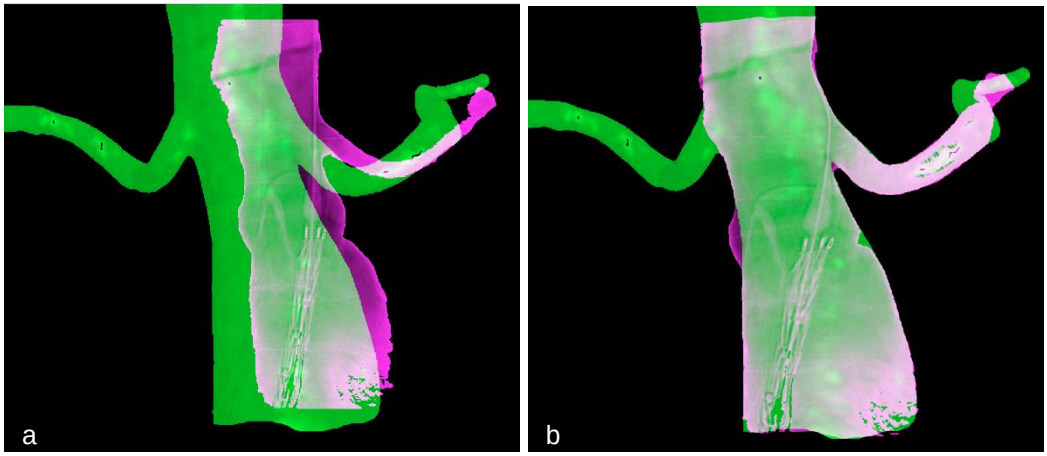

Figure 14 – Initial fusion (a) and improved fusion (b), this registration took 12 seconds and the mismatch measurements improved from 7.7 mm to 0.2 mm. CTA (green), DSA (purple).

Table 3: Deformable fusion results obtained with MatLab simulations

Registration	Number of iterations	Pyramid levels	Succes	Quality	Time (sec)	Mismatch (mm)
1	100	10	Yes	0.903	26	0.3
2	50	10	Yes	0.899	9	1
3	25	10	No	0.889	7	2.8
4	100	5	No	0.874	17	5.5
5	100	8	Yes	0.903	20	0.2
6	50	8	Yes	0.905	12	0.2
7	25	8	Yes	0.903	7	0.3
8	150	8	Yes	0.902	34	0.2
9	25	6	Yes	0.903	6	7.7
10	20	6	No	0.816	6	0.4

Table 3 displays the deformable fusion results. Seven of the ten registrations were successful, three registrations were not successful. The lowest mismatch was achieved in registrations 5,6 and 8 with registration times being 19, 12 and 34 seconds respectively. The fastest registration was registration 9 and 10 with 6 seconds. The slowest was registration 8 with 34 seconds.

8.3. Discussion

In this proof of concept investigation, we have demonstrated deformable fusion successfully with a highest accuracy of 0.2 mm. This was performed in a minimal time with fastest result being 6 seconds.
We have tried to find the boundary of accuracy versus time to perform. Since it would be ideal to find the highest accuracy in the lowest amount of time. Three registrations were not successful given the low amount of iterations and / or low value of the pyramid levels. Focusing on these values, the cut-off point between successful and unsuccessful deformable fusion would be 25 iterations and 6 pyramid levels. The time to perform with these settings is 6 seconds.

The challenge is to isolate the aorta from a DSA image. When DSA is performed, the image is different from patient to patient. The amount of iodine contrast and flow is different each time during DSA. A robust method must be developed how to isolate the aorta with renal artery branches after initial DSA.

It is important to implement deformable fusion in the clinical workflow as second step after the automated bone registration, as demonstrated in phase two of this paper. Given the 2D nature, it can be performed fast compared to a 3D registration.

Several successful attempts in literature are demonstrated. Lessard et al. has proposed a method to automatically detect selective arterial devices during EVAR.[47] Also, Breininger et al. has demonstrated intraoperative stent segmentation in X-ray fluoroscopy images during EVAR. [48] Additionally, Kaladji et al. have investigated the prediction of deformations during EVAR using finite element simulation.[49] With the knowledge of the location of the arterial devices and location of the stent, the fusion can be deformed to fit the device and stent.[50-53] When the preoperative CTA is fused with the patient to submillimetre level, this can provide the platform for future innovations such as a stent graft placement assistant, which can assist in the exact location deployment of the stent graft at the renal arteries.

8.4. Conclusion

In this proof of concept, deformable fusion was successful and accurate in one patient. Efforts to automate this technique is subject for future research. Besides the technical capabilities of image registration, an optimal contrast protocol should be chosen to ensure clear visualisation of the aorta and renal arteries.

9. GENERAL CONCLUSION

The aim was *to improve EVAR preoperative planning by evaluating automated and manual 3D sizing measurements and automated image fusion registration.*

In this study, we have demonstrated the evolvement of two techniques in the preoperative planning phase of EVAR. From phase one it can be concluded that all manual measurements resulted in an almost perfect agreement between both software programs. However when utilizing automated measurements, TR performed better compared to TR in terms of ICC value and mean difference per aortic measurement location.
From phase two it can be concluded that automated fusion between preoperative CTA and live fluoroscopy is feasible with a submillimetre bone mismatch. However, vascular mismatch was insufficient making automated image fusion on solely bony not applicable in a clinical setting without vascular mismatch correction.

10. RECOMMENDATIONS

Several recommendations can be made from this thesis. When focusing on the preoperative planning phase and comparison between AVA and TR, automation of measurements is still a field in which improvements can be made. When performing aortoiliac measurements, reliable automated diameters and lengths can make manual measurements obsolete. TR has demonstrated a reliable inner-to-inner functionality since it had an perfect agreement with the manual control group. For AVA, improvements of the automated measurements can make it more reliable and precise. Investigating the pixel and Hounsfield values showed it was likely AVA does not include pixel values in the intraluminal aorta close to the intima layer balancing around 100 HU. If AVA includes these regions, it is more likely an optimal intraluminal area is given by the automated functionality, without under sizing the inner-to-inner diameter. Categorising outer-to-outer diameters automatically is more challenging given the vessel wall is not iodinated by contrast. Techniques to overcome this could lie in the field of artificial intelligence by machine and deep learning. Pixel intensity differences which are difficult for the human eye to distinguish could be classified as vessel wall by an iterative process, learning from previous mistakes and successes.
For image fusion, if the 3D roadmap will follow the patient anatomy continuously, less nephrotoxic contrast and radiation can be used during the procedure since the surgeon relies more on the projected 3D roadmap. Adding to this is when performing the DSA and preoperative CTA, an optimal chosen contrast protocol should be chosen to ensure good visualisation of the arteries.
Furthermore, reliable automating as many steps as possible for image fusion will hypothetically result in a better workflow. Currently too many manual steps are needed which can impede a smooth clinical workflow if not practiced regularly. Vascular deformation after the insertion of a stiff guidewire and stent will keep on changing the anatomy of the patient intraoperatively. This is why it is important to develop an iterative automated image fusion workflow, in which the system corrects for vascular deformity regularly. Also it can be linked to a cloud platform and utilize artificial intelligence techniques to learn from previous anatomy deformations. If eventually a reliable and perfect match between preoperative CTA and the patient is reached, this can open the door for future techniques. Especially in complex EVAR, the stent graft positioning during the procedure is important to ensure a good clinical outcome. By developing smart software to assist the surgeon in stent positioning, it is hypothesised the stent graft positioning can be improved. This could assist as a clinical decision support tool.

REFERENCES

1. Kent KC. Clinical practice. Abdominal aortic aneurysms. *N Engl J Med.* 2014;371:2101-2108.

2. Sakalihasan N, Michel JB, Katsargyris A, et al. Abdominal aortic aneurysms. *Nature Review - Disease Primers.* 2018;4:34.

3. Nelissen BG, Herwaarden JA, Pasterkamp G, Moll FL, Vaartjes I. Shifting abdominal aortic aneurysm mortality trends in The Netherlands. *J Vasc Surg.* 2015;61:642-647 e642.

4. Powell JT, Sweeting MJ, Ulug P, et al. Meta-analysis of individual-patient data from EVAR-1, DREAM, OVER and ACE trials comparing outcomes of endovascular or open repair for abdominal aortic aneurysm over 5 years. *British Journal of Surgery.* 2017;104:166-178.

5. Mark J.W. Koelemay MHeACV. Richtlijn 'Diagnostiek en behandeling van het aneurysma van de abdominale aorta'. *Nederlands Tijdschrift Geneeskunde.* 2009.

6. Wanhainen A, Verzini F, Van Herzeele I, et al. European Society for Vascular Surgery (ESVS) 2019 Clinical Practice Guidelines on the Management of Abdominal Aorto-iliac Artery Aneurysms. *European Journal of Vascular and Endovascular Surgery.* 2018.

7. Daye D, Walker TG. Complications of endovascular aneurysm repair of the thoracic and abdominal aorta: evaluation and management. *Cardiovascular Diagnosis and Therapy.* 2018;8:S138-S156.

8. Malas MB, Freischlag JA. Interpretation of the results of OVER in the context of EVAR trial, DREAM, and the EUROSTAR registry. *Semin Vasc Surg.* 2010;23:165-169.

9. Powell JT, Sweeting MJ, Ulug P, et al. Meta-analysis of individual-patient data from EVAR-1, DREAM, OVER and ACE trials comparing outcomes of endovascular or open repair for abdominal aortic aneurysm over 5 years. *Br J Surg.* 2017;104:166-178.

10. Kristmundsson T, Sonesson B, Dias N, Tornqvist P, Malina M, Resch T. Outcomes of fenestrated endovascular repair of juxtarenal aortic aneurysm. *J Vasc Surg.* 2014;59:115-120.

11. Greenberg R, Eagleton M, Mastracci T. Branched endografts for thoracoabdominal aneurysms. *J Thorac Cardiovasc Surg.* 2010;140:S171-178.

12. de Almeida Sandri G, Ribeiro MS, Macedo TA, Vrtiska T, Oderich GS. Planning endovascular aortic repair with standard and fenestrated-branched endografts. *J Cardiovasc Surg (Torino).* 2017;58:204-217.

13. Rolls AE, Riga CV, Rudarakanchana N, et al. Planning for EVAR: the role of modern software. *J Cardiovasc Surg (Torino).* 2014;55:1-7.

14. Sobocinski J, Chenorhokian H, Maurel B, et al. The benefits of EVAR planning using a 3D workstation. *Eur J Vasc Endovasc Surg.* 2013;46:418-423.

15. Higashiura W, Sakaguchi S, Tabayashi N, Taniguchi S, Kichikawa K. Impact of 3-dimensional-computed tomography workstation for precise planning of endovascular aneurysm repair. *Circ J.* 2008;72:2028-2034.

16. Kaladji A, Lucas A, Kervio G, Haigron P, Cardon A. Sizing for endovascular aneurysm repair: clinical evaluation of a new automated three-dimensional software. *Ann Vasc Surg.* 2010;24:912-920.

17. Belvroy VM, Houben IB, Trimarchi S, Patel HJ, Moll FL, Van Herwaarden JA. Identifying and addressing the limitations of EVAR technology. *Expert Rev Med Devices.* 2018;15:541-554.

18. Huang IKH, Renani SA, Morgan RA. Complications and Reinterventions After Fenestrated and Branched EVAR in Patients with Paravisceral and Thoracoabdominal Aneurysms. *Cardiovasc Intervent Radiol.* 2018;41:985-997.

19. Lu YH, Mani K, Panigrahi B, Hsu WT, Chen CY. Endoleak Assessment Using Computational Fluid Dynamics and Image Processing Methods in Stented Abdominal Aortic Aneurysm Models. *Comput Math Methods Med.* 2016;2016:9567294.

20. Brewster DC, Cronenwett JL, Hallett JW, Jr., et al. Guidelines for the treatment of abdominal aortic aneurysms. Report of a subcommittee of the Joint Council of the American Association for Vascular Surgery and Society for Vascular Surgery. *J Vasc Surg.* 2003;37:1106-1117.

21. van Keulen JW, Moll FL, Tolenaar JL, Verhagen HJ, van Herwaarden JA. Validation of a new standardized method to measure proximal aneurysm neck angulation. *J Vasc Surg.* 2010;51:821-828.

22. Dua MM, Dalman RL. Hemodynamic influences on abdominal aortic aneurysm disease: Application of biomechanics to aneurysm pathophysiology. *Vascul Pharmacol.* 2010;53:11-21.

23. Macia I, Grana M, Maiora J, Paloc C, de Blas M. Detection of type II endoleaks in abdominal aortic aneurysms after endovascular repair. *Comput Biol Med.* 2011;41:871-880.

24. Varu VN, Greenberg JI, Lee JT. Improved efficiency and safety for EVAR with utilization of a hybrid room. *Eur J Vasc Endovasc Surg.* 2013;46:675-679.

25. Nguyen VL, Kooi ME, Backes WH, et al. Suitability of pharmacokinetic models for dynamic contrast-enhanced MRI of abdominal aortic aneurysm vessel wall: a comparison. *PLoS One.* 2013;8:e75173.

26. de Ruiter QM, Reitsma JB, Moll FL, van Herwaarden JA. Meta-analysis of Cumulative Radiation Duration and Dose During EVAR Using Mobile, Fixed, or Fixed/3D Fusion C-Arms. *J Endovasc Ther.* 2016;23:944-956.

27. de Ruiter QM, Gijsberts CM, Hazenberg CE, Moll FL, van Herwaarden JA. Radiation Awareness for Endovascular Abdominal Aortic Aneurysm Repair in the Hybrid Operating Room. An Instant Patient Risk Chart for Daily Practice. *J Endovasc Ther.* 2017;24:425-434.

28. de Ruiter QMB, Jansen MM, Moll FL, Hazenberg C, Kahya NN, van Herwaarden JA. Procedure and step-based analysis of the occupational radiation dose during endovascular aneurysm repair in the hybrid operating room. *J Vasc Surg.* 2018;67:1881-1890.

29. Ahmad W, Obeidi Y, Majd P, Brunkwall JS. The 2D-3D Registration Method in Image Fusion Is Accurate and Helps to Reduce the Used Contrast Medium, Radiation, and Procedural Time in Standard EVAR Procedures. *Ann Vasc Surg.* 2018;51:177-186.

30. Brina O, Ouared R, Bonnefous O, et al. Intra-aneurysmal flow patterns: illustrative comparison among digital subtraction angiography, optical flow, and computational fluid dynamics. *AJNR Am J Neuroradiol.* 2014;35:2348-2353.

31. Dias NV, Billberg H, Sonesson B, Tornqvist P, Resch T, Kristmundsson T. The effects of combining fusion imaging, low-frequency pulsed fluoroscopy, and low-concentration contrast agent during endovascular aneurysm repair. *J Vasc Surg.* 2016;63:1147-1155.

32. Dijkstra ML, Eagleton MJ, Greenberg RK, Mastracci T, Hernandez A. Intraoperative C-arm cone-beam computed tomography in fenestrated/branched aortic endografting. *J Vasc Surg.* 2011;53:583-590.

33. Hertault A, Maurel B, Sobocinski J, et al. Impact of hybrid rooms with image fusion on radiation exposure during endovascular aortic repair. *Eur J Vasc Endovasc Surg.* 2014;48:382-390.

34. Hertault A, Rhee R, Antoniou GA, et al. Radiation Dose Reduction During EVAR: Results from a Prospective Multicentre Study (The REVAR Study). *Eur J Vasc Endovasc Surg.* 2018;56:426-433.

35. Stangenberg L, Shuja F, Carelsen B, Elenbaas T, Wyers MC, Schermerhorn ML. A novel tool for three-dimensional roadmapping reduces radiation exposure and contrast agent dose in complex endovascular interventions. *J Vasc Surg.* 2015;62:448-455.

36. Koutouzi G, Sandstrom C, Roos H, Henrikson O, Leonhardt H, Falkenberg M. Orthogonal Rings, Fiducial Markers, and Overlay Accuracy When Image Fusion is Used for EVAR Guidance. *Eur J Vasc Endovasc Surg.* 2016;52:604-611.

37. Goudeketting SR, Heinen SGH, Unlu C, et al. Pros and Cons of 3D Image Fusion in Endovascular Aortic Repair: A Systematic Review and Meta-analysis. *J Endovasc Ther.* 2017;24:595-603.

38. Southerland KW, Nag U, Turner M, et al. Image-Based Three-Dimensional Fusion Computed Tomography Decreases Radiation Exposure, Fluoroscopy Time, and Procedure Time During Endovascular Aortic Aneurysm Repair. *Journal of Vascular Surgery.* 2018;67:e61.

39. Jones DW, Stangenberg L, Swerdlow NJ, et al. Image Fusion and 3-Dimensional Roadmapping in Endovascular Surgery. *Ann Vasc Surg.* 2018;52:302-311.

40. Maurel B, Martin-Gonzalez T, Chong D, et al. A prospective observational trial of fusion imaging in infrarenal aneurysms. *J Vasc Surg.* 2018;68:1706-1713 e1701.

41. Rolls AE, Maurel B, Davis M, Constantinou J, Hamilton G, Mastracci TM. A Comparison of Accuracy of Image- versus Hardware-based Tracking Technologies in 3D Fusion in Aortic Endografting. *Eur J Vasc Endovasc Surg.* 2016;52:323-331.

42. Liu Z, Deng X, Wang G-z. Accuracy Validation for Medical Image Registration Algorithms: a Review. *Chinese Medical Sciences Journal.* 2012;27:176-181.

43. Matl S, Brosig R, Baust M, Navab N, Demirci S. Vascular image registration techniques: A living review. *Med Image Anal.* 2017;35:1-17.

44. Fitzpatrick JM, West JB, Maurer CR, Jr. Predicting error in rigid-body point-based registration. *IEEE Trans Med Imaging.* 1998;17:694-702.

45. Raj Varadhan1, a, Grigorios Karangelis2, Karthik Krishnan3, and Susanta Hui4. A framework for deformable image registration validation in radiotherapy clinical applications. *J Appl Clin Med Phys.* 2013.

46. Truijers M, Resch T, Van Den Berg JC, Blankensteijn JD, Lonn L. Endovascular aneurysm repair: state-of-art imaging techniques for preoperative planning and surveillance. *J Cardiovasc Surg (Torino).* 2009;50:423-438.

47. Lessard S, Kauffmann C, Pfister M, et al. Automatic detection of selective arterial devices for advanced visualization during abdominal aortic aneurysm endovascular repair. *Med Eng Phys.* 2015;37:979-986.

48. Breininger K, Albarqouni S, Kurzendorfer T, Pfister M, Kowarschik M, Maier A. Intraoperative stent segmentation in X-ray fluoroscopy for endovascular aortic repair. *Int J Comput Assist Radiol Surg.* 2018;13:1221-1231.

49. Kaladji A, Dumenil A, Castro M, et al. Prediction of deformations during endovascular aortic aneurysm repair using finite element simulation. *Comput Med Imaging Graph.* 2013;37:142-149.

50. Gindre J, Bel-Brunon A, Rochette M, et al. Patient-Specific Finite-Element Simulation of the Insertion of Guidewire During an EVAR Procedure: Guidewire Position Prediction Validation on 28 Cases. *IEEE Trans Biomed Eng.* 2017;64:1057-1066.

51. Solbiati M, Passera KM, Goldberg SN, et al. A Novel CT to Cone-Beam CT Registration Method Enables Immediate Real-Time Intraprocedural Three-Dimensional Assessment of Ablative Treatments of Liver Malignancies. *Cardiovasc Intervent Radiol.* 2018;41:1049-1057.

52. Cercenelli L, Bortolani B, Tiberi G, et al. Characterization of Vessel Deformations During EVAR: A Preliminary Retrospective Analysis to Improve Fidelity of Endovascular Simulators. *J Surg Educ.* 2018;75:1096-1105.

53. Schwein A, Chinnadurai P, Behler G, Lumsden AB, Bismuth J, Bechara CF. Computed tomography angiography-fluoroscopy image fusion allows visceral vessel cannulation without angiography during fenestrated endovascular aneurysm repair. *J Vasc Surg.* 2018;68:2-11.

APPENDIX

Phase one supplementary material

Example 1: Proximal seal zone patient 5, D2A	
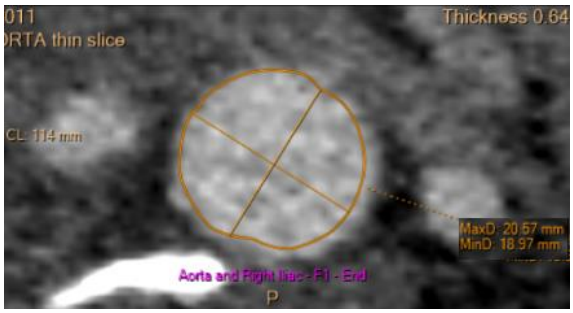	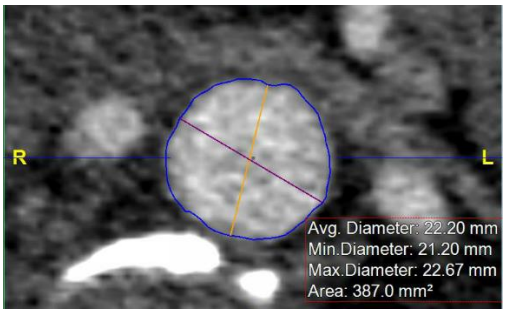
AVA, MaxD = 20.6 mm	TR, MaxD = 22.7 mm
Example 2: Proximal seal zone patient 7, D3A	
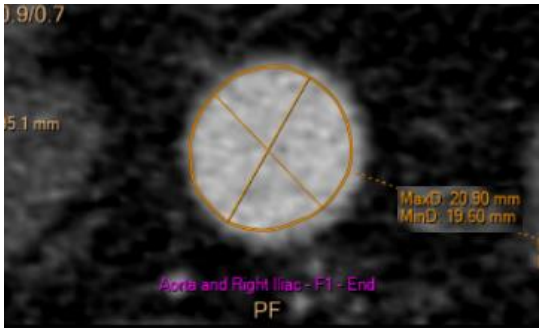	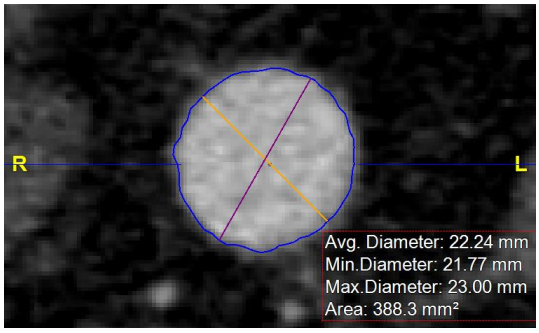
AVA, MaxD = 20.9 mm	TR, MaxD = 23.0 mm
Example 3: Distal seal zone patient 7, D11A	
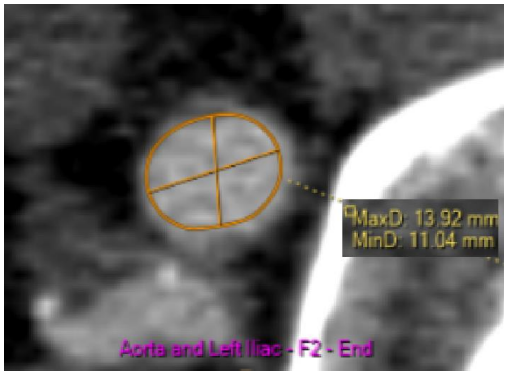	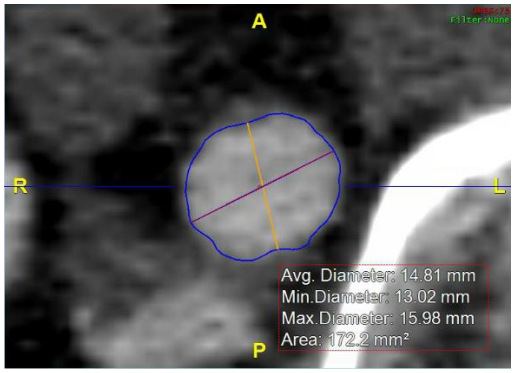
AVA, MaxD = 13.9 mm	TR, MaxD = 16.0 mm
Example 4: Proximal seal zone manual patient 7, D14M	
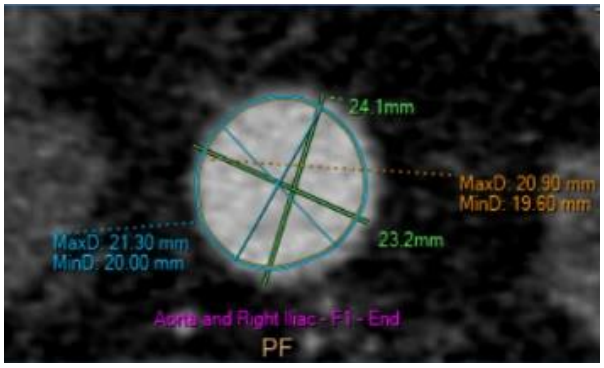	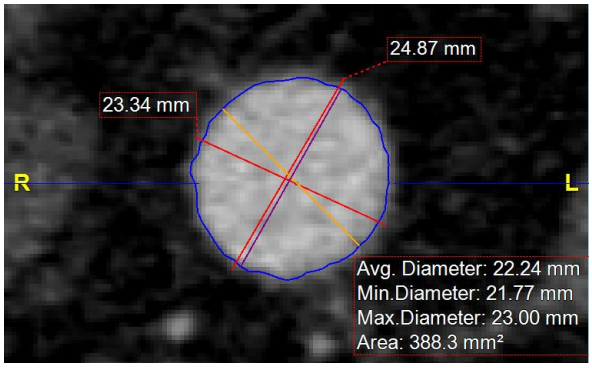
AVA, MaxD = 24.1 mm	TR, MaxD = 24.9 mm.

Example 5: Aortic length patient 5, L6M

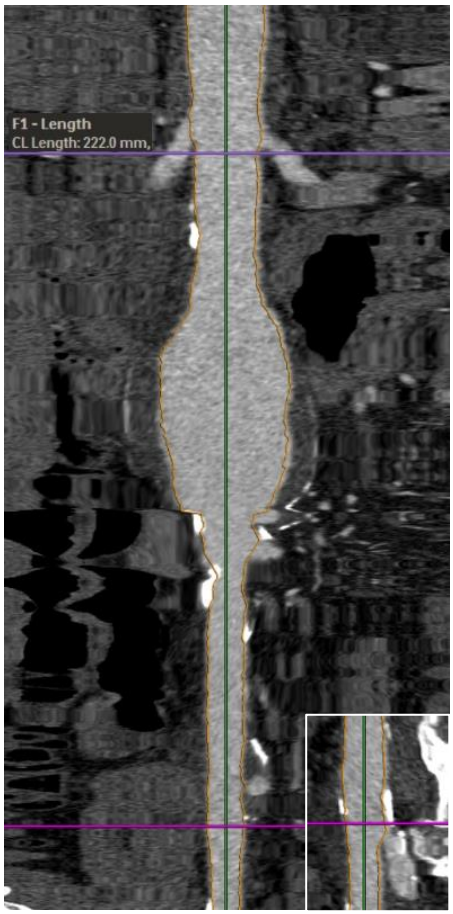

AVA, CL Length: 222.0 mm

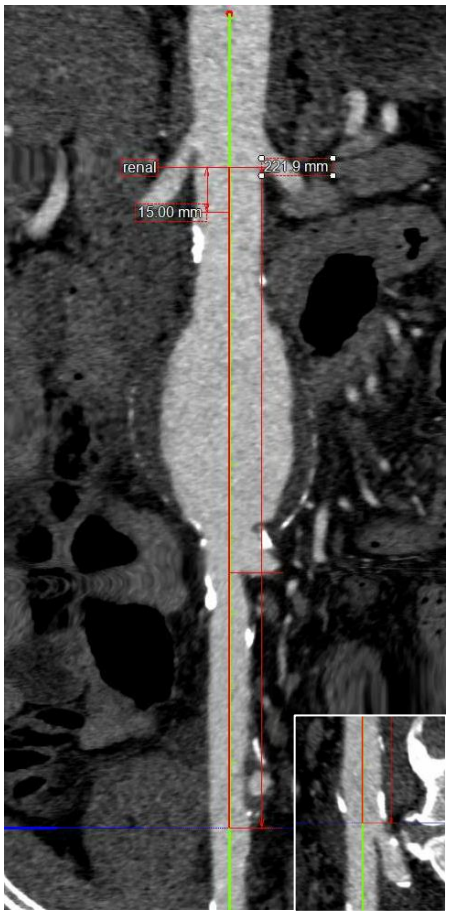

TR, CL Length: 221.9 mm

Example 6: Proximal seal zone patient 4, D14M with **thrombus**

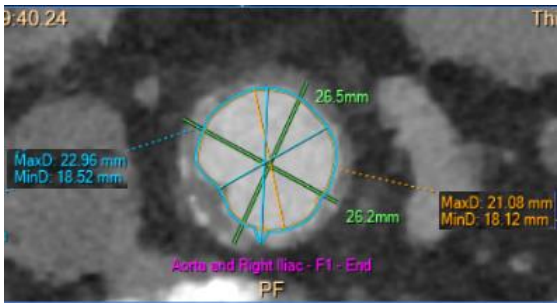

AVA, MaxD: 26.5 mm

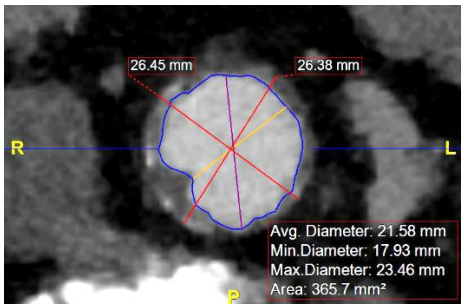

TR, maxD: 26.5 mm

Example 7: Proximal seal zone patient 6, D13M with **calcification**

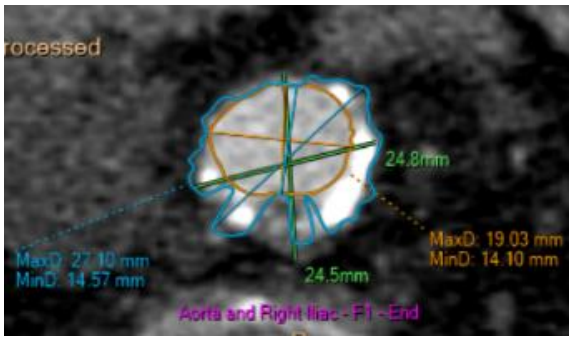

AVA, MaxD: 24.8 mm

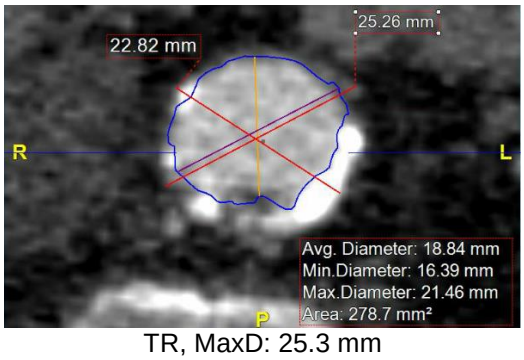

TR, MaxD: 25.3 mm

Phase two supplementary material

Patient 5 No complete vertebra pair was in the region of interest.	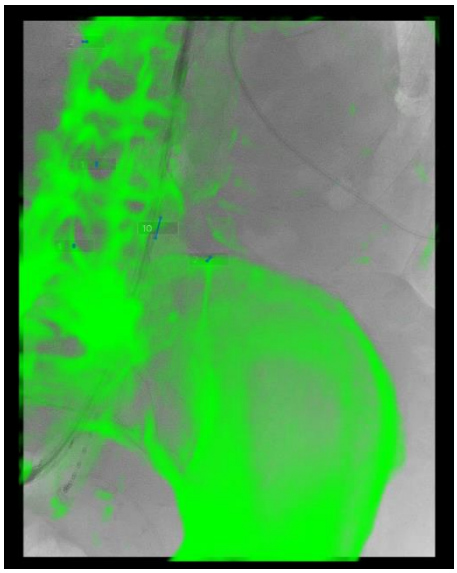
Patient 8 Macro view with many vertebra pairs visible.	
Patient 10 -	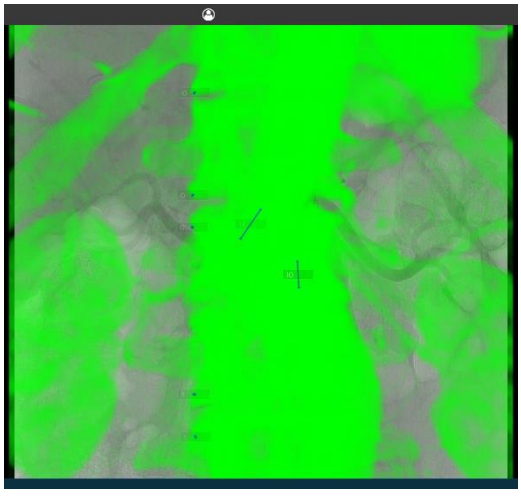

Manual adjustment was needed in patients 5-8 since no sufficient registration was given by the automated registration algorithm. The registration option ‘Guess’ was used in these cases.

LIST OF ABBREVIATIONS

3DWS	3 Dimensional Work Station
AAA	Abdominal Aortic Aneurysm
AVA	Advanced Vessel Analysis (Philips, Best, NL)
BEVAR	Branched Endovascular Aortic Aneurysm
CA	Celiac Artery / Trunk
CLL	Central Lumen Line
CTA	Computed Tomography Angiography
DSA	Digital Subtraction Angiography
EVAR	Endovascular Aortic Aneurysm
FEVAR	Fenestrated Endovascular Aortic Aneurysm
HU	Hounsfield (unit)
ICC	Interclass Correlation Coefficient
IFU	Instructions For Use
LRA	Left Renal Artery
RRA	Right Renal Artery
SD	Standard Deviation
SMA	Superior Mesenteric Artery
TR	TeraRecon Aquarius iNtuition (TR, Foster City, California, USA)

THESIS EXPERIENCE SUMMARY

PRESENTATIES ZIEKENHUIS

1. Werkplan 13-2-2019
2. Meeting Philips + Sr. Director Clinical Science Europe 7-5-2019
3. Preliminary Results 23-8-2019
4. Meeting Philips + Israel Delegatie 27-8-2019
5. Promotie rondleiding prof. Zweden 03-10-2019
6. College Hybride OK Cardiovascular Research Master 24-10-2019
7. Wetenschapsdag 15-11-2019
8. College Hybride OK CardioVascular Research Master 10-12-2019
9. Final Project Results @ Philips Best – 4-12-2019

PRESENTATIES INTERNATIONALE CONGRESSEN:

1. ESCVS Maart 2019 – GRONINGEN
   Poster Presentation
2. ESVS Aug 2019 - HAMBURG
   6 min fast-track presentation
3. EAST MEETS WEST Sept 2019 – BOEKAREST
   10 min presentation
4. ENDOVASCOLOGY Sept 2019 – SHANGHAI
   10 min presentation
   30 min presentation Shanghai Military University Hospital

PRIJZEN:

BEST VASCULAR POSTER AWARD ESCVS 2019 - €250

KLINISCH:

- Fuseren op hybride OK bij elke complexe EVAR
- Assisteren op OK tijdens EVAR
- 3D sizen van klinische EVAR patiënten, ook IBD (iliac-branch-device).
- Informed consent bij patienten.

EXTRA WERKZAAMHEDEN:

- METC niet-WMO aanvraag M3 project
- ZEPHYR study coordinator (observationele registry Cook endografts)
- SURPASS study coordinator (observationele registry Gore iliac branch device)
- AneuFix study coordinator (type 2 endoleak polymer filling prospective study)
- Research contract afsluiten Philips – VUmc.
- DCE MRI project MR intekenen (prof. Nederveen AMC)
- Begeleiden student geneeskunde wetenschappelijke stage (okt 2019)
- Website bouwen Amsterdam Open Vascular Aortic Course 2020

FIRST / CO-AUTEUR / REVIEWER

- Eerste auteur paper na M2-3 stage: *'Image Fusion during Standard and Complex Endovascular Aortic Repair, To Fuse or Not to Fuse? A Meta-analysis and Comparison with Single Centre Retrospective Data'*.
- ZONMW grant co-auteur: *'Early Detection and Treatment of Complications After Endovascular Repair of Abdominal Aortic Aneurysms with New Imaging Techniques'* Project: 10-10400-98-18013 (final round).
- Reviewer voor Nature Scientific Reports: *'Artificial intelligence in abdominal aortic aneurysm'*
- Reviewer voor Nature Scientific Reports: *'Artificial intelligence can better predict the postoperative death of abdominal aortic aneurysm'*